Effect of PIP_2 Binding on the Membrane Docking Geometry of PKCα C2 Domain: An EPR Site-Directed Spin-Labeling and Relaxation Study[†]

Kyle E. Landgraf, Nathan J. Malmberg, and Joseph J. Falke*

Department of Chemistry and Biochemistry and the Molecular Biophysics Program, University of Colorado, Boulder, Colorado 80309-0215

Received November 30, 2007; Revised Manuscript Received May 28, 2008

ABSTRACT: Protein kinase C isoform alpha (PKCα) is a ubiquitous, conventional PKC enzyme that possesses a conserved C2 domain. Upon activation by cytoplasmic Ca^{2+} ions, the C2 domain specifically binds to the plasma membrane inner leaflet where it recognizes the target lipids phosphatidylserine (PS) and phosphatidylinositol-4,5-bisphosphate (PIP_2). The membrane penetration depth and docking angle of the membrane-associated C2 domain is not well understood. The present study employs EPR site-directed spin labeling and relaxation methods to generate a medium-resolution model of the PKCα C2 domain docked to a membrane of lipid composition similar to the plasma membrane inner leaflet. The approach measures EPR depth parameters for 10 function-retaining spin labels coupled to the C2 domain, and for spin labels coupled to depth calibration molecules. The resulting depth parameters, together with the known structure of the free C2 domain, provide a sufficient number of constraints to define two membrane docking geometries for C2 domain bound to physiological membranes lacking or containing PIP_2, respectively. In both the absence and presence of PIP_2, the two bound Ca^{2+} ions of the C2 domain lie near the anionic phosphate plane in the headgroup region, consistent with the known ability of the Ca^{2+} and membrane-binding loops (CMBLs) to bind the headgroup of the PS target lipid. In the absence of PIP_2, the polybasic lipid binding site on the $\beta3$-$\beta4$ hairpin is occupied with PS, but in the presence of PIP_2 this larger, higher affinity target lipid competitively displaces PS and causes the long axis of the domain to tilt $40 \pm 10°$ toward the bilayer normal. The ability of the $\beta3$-$\beta4$ hairpin site to bind PS as well as PIP_2 extends the lifetime of the membrane-docked state and is predicted to enhance the kinase turnover number of PKCα during a single membrane docking event. In principle, PIP_2-induced tilting of the C2 domain could modulate the activity of membrane-docked PKCα as it diffuses between membrane regions with different local PS and PIP_2 concentrations. Finally, the results demonstrate that EPR relaxation methods are sufficiently sensitive to detect signaling-induced changes in the membrane docking geometries of peripheral membrane proteins.

Many diverse cell signaling processes rapidly modulate the levels of intracellular small molecule second messengers in order to spatially and temporally regulate the activity of downstream effectors. Important reactions on membrane surfaces are often stimulated by second messenger signals which recruit signaling enzymes to the appropriate membrane, thereby bringing these enzymes to their membrane-bound substrates. Such membrane recruitment is typically controlled by a membrane targeting domain activated by the binding of a second messenger, often a signaling lipid or cytoplasmic Ca^{2+}. One the most prevalent membrane targeting motifs is the C2 domain, which can be activated by Ca^{2+} binding and is widely found in membrane-targeted signaling proteins [reviewed in refs *1–8*]. In a typical cell, transient cytoplasmic Ca^{2+} signals recruit multiple C2 domain-containing proteins to specific intracellular membrane surfaces, thereby modulating crucial membrane-associated signaling pathways.

The conventional isoforms of protein kinase C (PKCα,[1] PKCβ and PKCγ) possess Ca^{2+}-activated C2 domains which recruit their parent proteins specifically to the inner leaflet of the plasma membrane where they phosphorylate membrane-bound substrate proteins [reviewed in refs *7, 9–13*]. Their shared topology consists of an N-terminal pseudosubstrate motif that provides kinase autoinhibition, followed by a pair of C1 domains that bind the signaling lipid diacylgycerol (DAG), then by a single plasma membrane-targeting C2 domain, and finally by the C-terminal kinase domain. The present study focuses on the C2 domain of the conventional PKCα protein, which binds two Ca^{2+} ions and associates with two lipids essential for its plasma membrane targeting: phosphatidylserine (PS), the most abundant anionic lipid of the plasma membrane; and phosphatidylinositol-4,5-bisphosphate (PIP_2), the most abundant phosphorylated PIP lipid (*14–24*). The activation of conventional PKCs has been

[†] Support provided by NIH R01 GM-063235 (to J.J.F.).

* To whom correspondence should be addressed. E-mail: falke@colorado.edu. Tel: (303) 492-3503. Fax: (303) 492-5894.

[1] Abbreviations: PKCα, protein kinase C, alpha isoform; CMBL, Ca^{2+}- and membrane-binding loop; PC, phosphatidylcholine; PS, phosphatidylserine; PE, phosphatidylethanolamine; dPE, dansyl-PE; PIP_2, phosphatidylinositol-4,5-bisphosphate; DTT, dithiothreitol; EDTA, ethylene diamine tetraacetic acid.

10.1021/bi800711t CCC: $40.75
Published on Web 07/09/2008

described as a sequential process in which, following a transient Ca^{2+} signal, the Ca^{2+}-occupied C2 domain first associates with plasma membrane PS and PIP_2, thereby allowing the C1 domains to search for the more rare DAG messenger (*11, 24, 25*). Ultimately, the simultaneous binding of the C1 and C2 domains to their lipid targets displaces the pseudosubstrate from the kinase active site. The ensuing loss of autoinhibition, together with close proximity to membrane-bound substrates, provides dual activation of the kinase domain.

High resolution X-ray crystal structures are available for PKCα C2 domain and several of its complexes (*16, 26*). As for other C2 domains, the core of this domain is an eight-stranded antiparallel β-sandwich. At one edge of the sandwich lie three interstrand Ca^{2+}- and membrane-binding loops (CMBL1−3). The crystal structure of a complex between PKCα C2 domain and the PS headgroup reveals that the two bound Ca^{2+} ions chelated by CMBL1−3 also receive direct and indirect coordination from the 1-phosphate of the PS headgroup (*16*), indicating that the Ca^{2+} binding site is central to PS recognition and binding. In addition, the structure of a different PS complex shows that a basic cluster of four lysine residues (K197, K199, K209, K211), all located on the β3-β4 hairpin, directly contacts a second PS headgroup, indicating that this basic cluster serves as a second binding site for anionic lipics such as PS (*26*). Recently, it has been established that the lysine cluster binds PIP_2 with higher affinity than PS, and that PIP_2 binding is essential for high affinity membrane docking *in vitro* as well as specific plasma membrane targeting in live cells (*20, 22–24*).

Despite advances in the structural analysis of isolated PKC C2 domains, the structures of their membrane-docked states remain poorly described. Of particular interest for the conventional PKC C2 domains is a structural understanding of their simultaneous docking to its two target lipids, PS and PIP_2, on a bilayer surface. Currently, high resolution methods are not yet capable of analyzing the structures of peripheral proteins docked to lipid bilayers, thus medium resolution approaches must be employed to generate molecular pictures of peripheral proteins in their active, membrane-bound states. In recent years, an EPR approach involving site-directed spin labeling and spin relaxation measurements (*27–29*) has been shown to be an effective method for elucidating membrane docking geometries, and has been successfully applied to several C2 domains (*30–35*). The docking geometry provided by EPR analysis, in turn, can serve as an experimentally defined starting point for subsequent molecular dynamics simulations designed to develop atomic resolution models of the membrane-docked protein (*36*). Previously, in an initial study of the PKCα C2 domain, we used EPR and fluorescence spectroscopies to identify the membrane docking surfaces, and to develop a preliminary model for the membrane docking geometry (*37*). The resulting model of this C2 domain docked to 3:1 PC:PS membranes suggested that the CMBLs penetrate the headgroup region of the bilayer, while a cluster of lysine residues lies near the surface of the headgroup region. However, the simplified lipid mixture used in the model target membranes lacked the important target lipid PIP_2 as well as other lipids found in the inner leaflet of the plasma membrane. Moreover, this previous study employed a low density of spin label positions on the membrane docking surface, yielding only a preliminary, qualitative picture of the membrane docking geometry.

The present study utilizes EPR site-directed spin labeling and relaxation techniques to generate the first medium resolution structural model of the PKCα C2 domain docked to a lipid bilayer composed of a physiological mixture of lipids. Specifically, the membrane penetration depth and docking angle are determined for the C2 domain bound to physiological membranes lacking or containing the target lipid PIP_2. The results provide the first molecular view of a peripheral membrane protein simultaneously docked to two target lipids, thereby significantly extending our mechanistic understanding of the dual lipid specificity required for plasma membrane targeting by conventional PKC C2 domains. Moreover, the findings reveal that PIP_2 binding to the lysine cluster significantly alters the membrane docking geometry of the C2 domain by tilting the domain relative to the membrane surface. This advance demonstrates that the EPR approach can be used to analyze changes in membrane docking geometry triggered by protein switching between different functional states. Finally, the results imply that target lipid-triggered geometry changes could play an important role in modulating the bound state lifetime and function of membrane-bound, conventional PKCs.

MATERIALS AND METHODS

Reagents. All lipids were synthetic unless otherwise indicated. 1-Palmitoyl-2-oleoyl-*sn*-glycero-3-phosphocholine (phosphatidylcholine, POPC, PC); 1-palmitoyl-2-oleoyl-*sn*-glycero-3-phosphoethanolamine (phosphatidylethanolamine, POPE, PE); 1-palmitoyl-2-oleoyl-*sn*-glycero-3-phosphoserine (phosphatidylserine, POPS, PS); L-α-phosphatidylinositol (PI) natural from bovine liver; L-α-phosphatidylinositol-4,5-bisphosphate ($PI(4,5)P_2$, PIP_2) natural from porcine brain; and sphingomyelin (SM) natural from brain were all purchased from Avanti Polar Lipids. Cholesterol (CH) was from Sigma. *N*-[5-(Dimethylamino)naphthalene-1-sulfonyl]-1,2-dihexadecanoyl-*sn*-glycero-3-phosphoethanolamine (dansyl-PE, dPE) was from Molecular Probes. 1-Oxyl-2,2,5,5-tetramethyl-Δ^3-pyrroline-3-methylmethanethiosulfonate (MTSSL, R1) was from Toronto Research Chemicals. Ni^{2+}-ethylenediamine diacetic acid (NiEDDA) was formed by dissolving 17 mM ethylenediamine diacetic acid (EDDA) and 17 mM $Ni(OH)_2$ (both from Sigma) in water at 60 °C. This solution was filtered, lyophilized, resuspended in ethanol, and filtered again to remove unreacted material.

Protein Mutagenesis, Expression, and Purification. Single cysteine mutants of the C2 domain of human PKCα (residues 155−293 (*16*)) were generated using the Quick Change II XL (Stratagene) site-directed mutagenesis kit according to the manufacturer's protocol. All mutations were verified by sequencing of the entire C2 domain. The wild type and mutant versions of the C2 domain were expressed as His-tagged fusions in *Escherichia coli* BL21 cells. Transformed cells were grown at 37 °C to OD 0.6 and induced with 500 μM IPTG. After induction cells were grown at 30 °C for 8 h. Protein was bound on a Ni-NTA agarose affinity column, washed with 50 mM imidazole, and labeled with 1 mM MTSSL via a disulfide exchange reaction. Following labeling, bound protein was washed and eluted off the column by cleavage of the N-terminal His-tag with thrombin.

Thrombin was affinity extracted from the protein sample using p-aminobenzamidine resin (Sigma).

Preparation of Lipid Mixtures and Phospholipid Vesicles. All lipid components were mixed in solvent containing chloroform/methanol/water (1/2/0.8) to give the desired lipid ratios (below), dried under vacuum to remove all solvents, and then hydrated in assay buffer (25 mM *N*-(2-hydroxyethyl)piperazine-*N*′-2-ethanesulfonic acid (HEPES) at pH 7.4 with KOH, 140 mM KCl, 15 mM NaCl, and 0.5 mM $MgCl_2$) by rapid vortexing. Small unilamellar vesicles (SUV) were generated by sonication of the hydrated lipid mixture to clarity with a Misonix XL2020 probe sonicator. Vesicles used in the FRET assays were prepared with a total lipid concentration of 3 mM with mole percentages for physiological membrane mimics as previously described (*24*): PM(−)PIP_2, PE/PC/PS/PI/SM/CH/dPE (29.5/10.5/21/4.5/4.5/25/5); and PM(+)PIP_2, PE/PC/PS/PI/SM/CH/dPE/PIP_2 (27.5/10.5/21/4.5/4.5/25/5/2). See Table 1 (Results) for a summary of these mixtures. Stock vesicle solutions for EPR experiments were prepared with a total lipid concentration of 120 mM using the following mole percentages: PM(−)PIP_2, PE/PC/PS/PI/SM/CH (34.5/10.5/21/4.5/4.5/25); and PM(+)PIP_2, PE/PC/PS/PI/SM/CH/PIP_2 (32.5/10.5/21/4.5/4.5/25/2). The dansyl-PE (dPE) component was removed from the EPR mixtures and replaced with an equivalent mole percentage of PE. Following sonication, vesicle stocks were allowed to equilibrate overnight at 4 °C.

Measurement of Ca^{2+}-Dependent Membrane Binding. A protein-to-membrane fluorescence resonance energy transfer (FRET) assay was employed based on previously established methods (*17, 38, 39*). Briefly, samples were made containing C2 domain (0.2 μM) and either PM(−)PIP_2 or PM(+)PIP_2 membranes (200 μM total lipid, 100 μM accessible) in assay buffer (25 mM HEPES at pH 7.4 with KOH, 140 mM KCl, 15 mM NaCl, and 0.5 mM $MgCl_2$). Additionally, 0.15 mM EDTA was included in these samples to reduce the levels of contaminating Ca^{2+} from low micromolar to nanomolar. Sufficient Ca^{2+} was added in excess of EDTA to achieve concentrations of 10 μM, 100 μM, and 1 mM, and protein-to-membrane FRET was measured. Desired Ca^{2+} concentrations were determined using Maxchelator (www.stanford.edu/~cpatton/maxc.html). Fluorescence of the samples was measured in a Photon Technologies International spectrofluorimeter (QM-2000-6SE) at 25 °C, with excitation and emission slits at 4 and 8 nm, respectively. Intrinsic tryptophan residues in the C2 domain were excited at 284 nm, and the dansyl-PE emission at 522 nm was measured. The protein-to-membrane FRET was determined by subtraction of the background fluorescence due to direct excitation of dansyl-PE from the total fluorescence of a parallel control sample lacking Ca^{2+}. Other control experiments indicated that Ca^{2+} had no effect on the background dansyl-PE emission under these conditions.

EPR Spectra. EPR spectra were acquired using a Bruker ESP300E X-band spectrometer (9.4 GHz) equipped with a loop gap resonator (Medical Advances) as previously described (*32*). Briefly, samples contained 10−200 μM spin-labeled C2 domain along with (i) Ca^{2+} (1 mM), (ii) Ca^{2+} (1 mM) and PM(−)PIP_2 membranes (40 mM total lipid), or (iii) Ca^{2+} (1 mM) and PM(+)PIP_2 membranes (40 mM total lipid) in assay buffer (see previous section). A minimum of three 100 G scans were acquired at 23 °C with an incident power of 2.0 mW. Spectra obtained for the same spin labeled protein under different membrane conditions were measured on the same day with all sample parameters the same, including protein concentration, except for the membrane conditions as specified. The high concentration of membrane lipid used in all membrane-containing EPR samples (40 mM total, or approximately 20 mM accessible) is sufficient to ensure a low surface density of bound C2 domain, thereby preventing spin−spin interactions. For different spin labeled variants, the protein concentration varied within the indicated range, but spectra were normalized to the same total number of spins to account for differences in spin label concentrations. Moreover, studies of the same spin labeled protein at different concentrations within the indicated range yielded indistinguishable spectral line shapes, confirming the success of the experimental design. This design has proven effective in previous EPR studies of membrane docked C2 domains (*30–32, 34, 35, 37*). Finally, control studies indicate that nonspecific binding to membranes lacking target lipids PS and PIP_2 is negligible under these conditions (Figure 3C); thus, the present EPR studies monitor native binding of PKCα C2 domain to its membrane-associated target lipids.

EPR Power Saturation Measurements. To perform the power saturation measurements EPR samples were placed in TPX capillaries (Medical Advances) to allow for gas perfusion. Power saturation measurements were performed on each sample under three conditions: (i) in the presence of 10 mM NiEDDA and equilibrated for 15 min under nitrogen, (ii) in house air (20% O_2), and (iii) equilibrated for 15 min under nitrogen in the absence of any paramagnetic species. Each spectrum was obtained in two 2 min scans over 10 G (about the central resonance $m_I = 0$) at powers ranging from 0.2 to 80 mW. The amplitudes were plotted as a function of microwave power and fit to the following equation as previously described (*27, 33*):

$$A = CP^{1/2}[1 + (2^{-\varepsilon}+1)P/P_{1/2}]^{-\varepsilon} \quad (1)$$

where A is the peak-to-peak amplitude of the central resonance, C is a scaling factor, P is the microwave power, $P_{1/2}$ is the power at which half-saturation occurs, and ε is the a measure of homogeneity of saturation. The best-fit $P_{1/2}$ values were then used to calculate the collision, or accessibility, parameters for oxygen ($\Pi(O_2)$) and NiEDDA (Π(NiEDDA)) as described (*27, 33*):

$$\Pi(X) = [P_{1/2}(X)/\Delta H_{pp}(X) - P_{1/2}(N_2)/\Delta H_{pp}(N_2)]/[P_{1/2}(DPPH)/\Delta H_{pp}(DPPH)] \quad (2)$$

where X is either O_2 or NiEDDA, $P_{1/2}$ is the half-saturating power, and ΔH_{pp} is the peak-to-peak line width. The accessibility parameter was normalized to a solid sample of (1,1-diphenyl-2-picrylhydrazyl) to correct for spectrometer differences. Subsequently, the accessibility parameters for O_2 and NiEDDA were used to calculate depth parameters as previously described (*27, 33*):

$$\Phi = \ln(\Pi(O_2)/\Pi(\text{NiEDDA})) \quad (3)$$

where Φ is the measured depth parameter for each spin labeled site. Our analysis of membrane docking focuses mainly on depth parameters, rather than the corresponding accessibility parameters, because the depth parameter is less sensitive to variations in local steric factors, sample varia-

tions, and instrumental fluctuations under the conditions of our measurements. We calculate depth parameters from the ratio of O_2 and NiEDDA accessibility parameters measured on the same day. Thus, steric factors, which typically alter both accessibility parameters in similar ways, tend to cancel out in the ratio, as do sample and instrumental factors that similarly affect accessibility parameters measured on the same day.

Determination of Membrane Docking Geometry Using the Measured Depth Parameters. The following procedure was used to generate the optimized docking geometries from the 1dsy crystal structure coordinates. All 10 positions used for EPR depth parameter measurements were mutated to cysteine residues in the crystal structure and linked to the R1 spin label through a disulfide bond using the Biopolymer module of Insight2000 (Accelrys). All side chain conformations of the R1 spin labels were adjusted to dihedral angles of (g^+, g^+) or (+300°, +300°) about the first two side chain bonds. This configuration is the most commonly observed side chain conformation in crystal studies of the T4 lysozyme (*40*). Subsequently, the conformations of T214R1, L219R1 and R249R1 were modified to relieve steric clash with the peptide backbone, yielding (g^+, t) (+300°, 180°) for T214R1 and L219R1, and (t, g^+) (180°, +300°) for R249R1. Both of these alternative conformations are accepted configurations of the MTSSL side chain (*30, 32, 34, 40*). Subsequently, the coordinates of the nitroxide nitrogens were tabulated relative to the center of mass of the 1dsy structure in order to define each R1 in the docking models.

The docking geometry and penetration depth of the C2 domain were calculated by iterative fitting of the spin label depth parameters to an equation that models the dependence of the depth parameter on distance from the membrane center as a hyperbolic function (*33*):

$$\Phi = [L + B + \{(L - B)^2 + C^2\}^{1/2}]/2 \quad (4)$$

where B represents the depth parameter value for a spin label distant from the center of the membrane and C defines the curvature of the function at the transition between linear and constant dependence of the depth parameter on distance. L describes the linear behavior of the depth parameter observed for spin labels in the membrane interior:

$$L = m(x \sin\theta_z + y \cos\theta_z \cos\theta_x - z \cos\theta_z \sin\theta_x + PY_{trans} + D) + I \quad (5)$$

The m and I parameters represent the slope and intercept of the linear relationship. The x, y, and z coordinates tabulated from the nitoxide nitrogens of each spin label are represented by their respective letters, and the associated θ_x and θ_z variables represent rotations about the x- and z-axes of the coordinate system belonging to the nitroxide nitrogens. P is a Boolean variable set to unity for protein spin labels or zero for the calibration spin labels. D represents the known membrane depth of the spin-label, which is nonzero only for the calibration spin-labels. Altogether the equation used for fitting possesses one dependent variable (Φ), five independent variables (x, y, z, P and D) and seven unknown variables (θ_x, θ_z, Y_{trans}, m, I, B and C). Nonlinear least-squares fitting of eq 4 was performed using Igor Pro (Wavemetrics), yielding best-fit values of θ_x, θ_z, Y_{trans}, m, I.

The algorithm used during the iterative fitting recognizes a laboratory axis system where the origin (0, 0, 0) is at the center-of-mass of the 1dsy structure and the x- and y-axes are horizontal and vertical, respectively, in the viewing plane. An imaginary phosphate plane is defined in this axis system as the x-z plane which passes through the origin (0, 0, 0), therefore the C2 domain begins partially imbedded in the membrane interior. Subsequently, rotations about the x- and z-axes, θ_x and θ_z, along with a y-axis translation, are performed to optimize the docking angle and penetration with respect to the imaginary phosphate plane, which remains fixed during the transformations. Note that due to the planar symmetry of the membrane, translations along the x- or z-axis as well as rotations about the y-axis result in no change to the docking geometry of the two models.

The final optimized transformations, which yielded the best fits shown in Figure 5, can be carried out on the PKCα C2 domain crystal structure (1dsy) to generate the best-fit docking models in the absence and presence of PIP_2. All rotations are performed from the perspective of an observer looking down the positive x- or z-axis toward the origin. Specifically, to generate the docking model in the absence of PIP_2, the crystal structure (1dsy) was rotated counterclockwise 260° (uncertainty ± 10°) about the x-axis, then counterclockwise 37° (uncertainty ± 7°) about the z-axis, followed by a translation of −7.7 Å (uncertainty ± 2.8 Å) along the y-axis to achieve a hyperbolic best-fit with a correlation coefficient $R = 0.99$. To generate the model for C2 domain docking to membranes containing PIP_2, the crystal structure was rotated counterclockwise 226° (uncertainty ± 22°) about the x-axis, then counterclockwise 70° (uncertainty ± 3°) about the z-axis, followed by a translation of −15.8 Å (uncertainty ± 2.3 Å) along the y-axis, yielding a hyperbolic best-fit with a correlation coefficient of $R = 0.99$. Finally, to produce Figures 5 and 6 a rotation counterclockwise of 180° about the y-axis was carried out to provide a clear view of the PIP_2-induced tilt.

RESULTS

Strategy. The goals of this study are to characterize the membrane docking geometry of the PKCα C2 domain bound to synthetic membranes that mimic the inner leaflet of the plasma membrane, and to determine the effect of the target lipid phosphatidylinositol-4,5-bisphosphate (PIP_2) on docking geometry. Previously, we have used fluorescence and spin-label EPR methods to qualitatively probe the geometry and depth of membrane penetration of the PKCα C2 domain bound to synthetic bilayer membranes containing phosphatidylcholine (PC) and the target lipid phosphatidylserine (PS) in a PC:PS mole ratio of 3:1 (*37*). However, in addition to PC and PS, the native plasma membrane inner leaflet possesses phosphatidylinositol-4,5-bisphosphate (PIP_2) and other lipids. PIP_2, like PS, is a target lipid of the PKCα C2 domain and is essential for specific recruitment to the plasma membrane (*20, 22, 24*). The present study thus employs a physiological mixture of lipids closely mimicking the composition of the plasma membrane inner leaflet (*24*) to analyze the docking geometry of the PKCα C2 domain bound to its native target membrane, and to test for PIP_2-induced changes in docking geometry.

In contrast to our previous spin-label EPR study which scattered spin-label positions at a low density over the entire

Table 1: Lipid Composition of Plasma Membrane-Mimicking Membranes[a]

lipid	abbreviation	mol % PM(−)PIP_2	mol % PM(+)PIP_2
1-palmitoyl-2-oleoyl-*sn*-glycero-3-phosphatidylethanolamine	PE	29.5	27.5
1-palmitoyl-2-oleoyl-*sn*-glycero-3-phosphatidylcholine	PC	10.5	10.5
1-palmitoyl-2-oleoyl-*sn*-glycero-3-phosphatidylserine	PS	21	21
L-α-phosphatidylinositol	PI	4.5	4.5
sphingomyelin	SM	4.5	4.5
cholesterol	CH	25	25
L-α-phosphatidylinositol-4,5-bisphosphate	PIP_2		2
1,2-dihexadecanoyl-*sn*-glycero-3-dansyl-phosphatidylethanolamine	dPE	5	5

[a] The indicated lipid compositions are designed to mimic the plasma membrane inner leaflet (*24*), either lacking or containing the target lipid PIP_2. Estimates of total PIP_2 in the plasma membrane inner leaflet range from 2 (*24, 50*) to over 5 (*51*) mol %. However, the free PIP_2 available for PKCα C2 domain binding will be lower due to the presence of other PIP_2 binding proteins (*12*). Thus, we employed 2 mol % of PIP_2 to approximate the level of free PIP_2 under cellular conditions. For EPR measurements, the FRET acceptor dPE was replaced with the same mole percentage of PE.

surface of the PKCα C2 domain (*37*), the present study concentrates nearly all spin-labels within the membrane docking surface. This approach yields a 2-fold higher density of spin-label probes in the region relevant to geometry measurements, and thereby significantly enhances the accuracy of the final geometry determination. Altogether, 14 spin-labeling sites are analyzed in the present study, and spin-labels at 10 of these sites are found to retain near-native, Ca^{2+}-dependent binding to membranes containing PS and PIP_2. EPR studies of the 10 functional spin-labeled proteins reveal spectral changes upon membrane docking, and further spectral changes are observed at certain spin-label positions when PIP_2 is included in the membranes. Similarly, EPR membrane depth parameters reveal PIP_2-induced depth changes at certain positions. Together, the EPR data define the different geometries of PKCα C2 domain docked to membranes containing either one (PS) or both (PS and PIP_2) of its target lipids, thereby characterizing the two predominant physiological docking states of this C2 domain.

Site-Selection, Mutagenesis and Spin-Labeling of the PKCα C2 Domain. To quantitate the membrane docking geometry of the PKCα C2 domain we selected (i) 8 positions for spin-labeling within the 3 loops that bind Ca^{2+} and PS, (ii) 5 positions within the PIP_2 binding site, and (iii) 1 control position distal from the membrane docking face. Figure 1 summarizes the locations of the 14 selected positions in the known PKCα C2 domain crystal structure (*16*). Each selected position was mutated to cysteine using site-directed mutagenesis, yielding a unique labeling site since the PKCα C2 domain contains no intrinsic cysteines. To generate the purified, spin-labeled proteins each mutant was expressed as a His-tag fusion in *E. coli* and affinity purified on a Ni-NTA column. The column-bound protein was labeled with the methanethiolsulfonate spin-label (MTSSL), hereafter designated R1, and was then eluted from the column by cleavage of the His-tag with thrombin. The thrombin protease was affinity extracted from the eluted samples, and each concentrated, R1-labeled mutant was found to be >95% pure

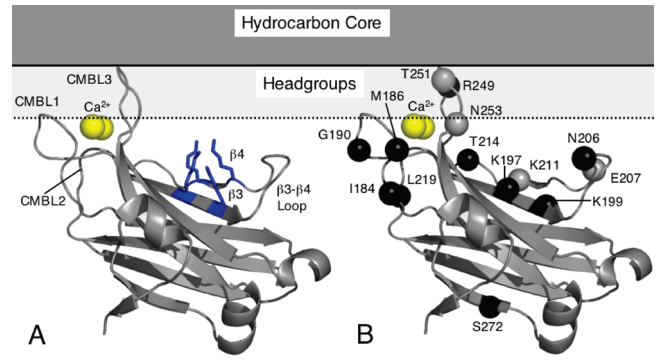

FIGURE 1: The PKCα C2 domain and positions chosen for spin-labeling. Shown is the secondary structure of the PKCα C2 domain (crystallographic coordinates 1dsy (*16*)) generated in Pymol (DeLano Scientific LLC). (A) Domain topology, illustrating the qualitative docking model defined by a previous study (*37*). The membrane docking face, which is the focus of the present study, includes the Ca^{2+}- and PS-binding loops (CMBLs 1, 2, and 3) and the PIP_2 binding site (the blue, 4-lysine cluster) located on the $\beta3$-$\beta4$ hairpin. The 2 bound Ca^{2+} ions are shown in yellow. (B) Sites selected for spin-labeling. The high density of probe positions on the membrane docking face allows for optimal EPR analysis of the docking geometry. Positions where spin-labeling caused serious loss of function, which were excluded from EPR studies, are shown in gray, leaving 10 positions shown in black for EPR analysis.

by SDS−PAGE. To test the function of these spin-labeled variants a protein-to-membrane FRET assay was employed to analyze Ca^{2+}-dependent membrane docking.

Effect of Spin-Labeling on Ca^{2+}-, PS-, and PIP_2-Dependent Membrane Binding. In order to identify perturbed spin-labeled variants possessing defects that could perturb the structure of their membrane-docked states, the membrane binding of each variant was tested under conditions designed to detect even minor losses of target lipid specificity or affinity. We have previously shown that at micromolar Ca^{2+} concentrations the PKCα C2 domain requires both PS and PIP_2 for high affinity membrane docking, while at millimolar Ca^{2+} PS alone is sufficient (*24*). Thus, to quantitate the membrane docking of the spin-labeled domains under conditions that required simultaneous recognition of Ca^{2+}, PS and PIP_2, a protein-to-membrane FRET assay (*38, 39*) was developed using Ca^{2+} concentrations ranging from 10 μM to 1 mM. The assay employed a mixture of lipids designed to mimic the lipid composition of the plasma membrane inner leaflet, containing the following components: phosphatidylethanolamine (PE), phosphatidylcholine (PC), phosphatidylserine (PS), phosphatidylinositol (PI), sphingomeylin (SM), and cholesterol (CH) (Table 1). Two parallel stocks of these membranes, designated PM(−)PIP_2 and PM(+)PIP_2 were generated, both of which contained equal, physiological levels of the target lipid PS (21 mol %), while either lacking or containing the physiological level of PIP_2 (0 or 2 mol %) (*24, 50*). Addition of PIP_2 was matched by a corresponding decrease in PE (29.5 to 27.5 mol %), so that all other lipid mole fractions remained constant. All membranes contained 5 mol % dansyl-phosphatidylethanolamine (dansyl-PE) to serve as a FRET acceptor. Previous studies have shown that changes in the PE mole ratio of the magnitude employed here, and the inclusion of 5 mol % dansyl-PE in the lipid mixtures, have no detectable effect on the membrane docking of C2 domains (*17, 24, 38, 39, 41*). The resulting membranes were

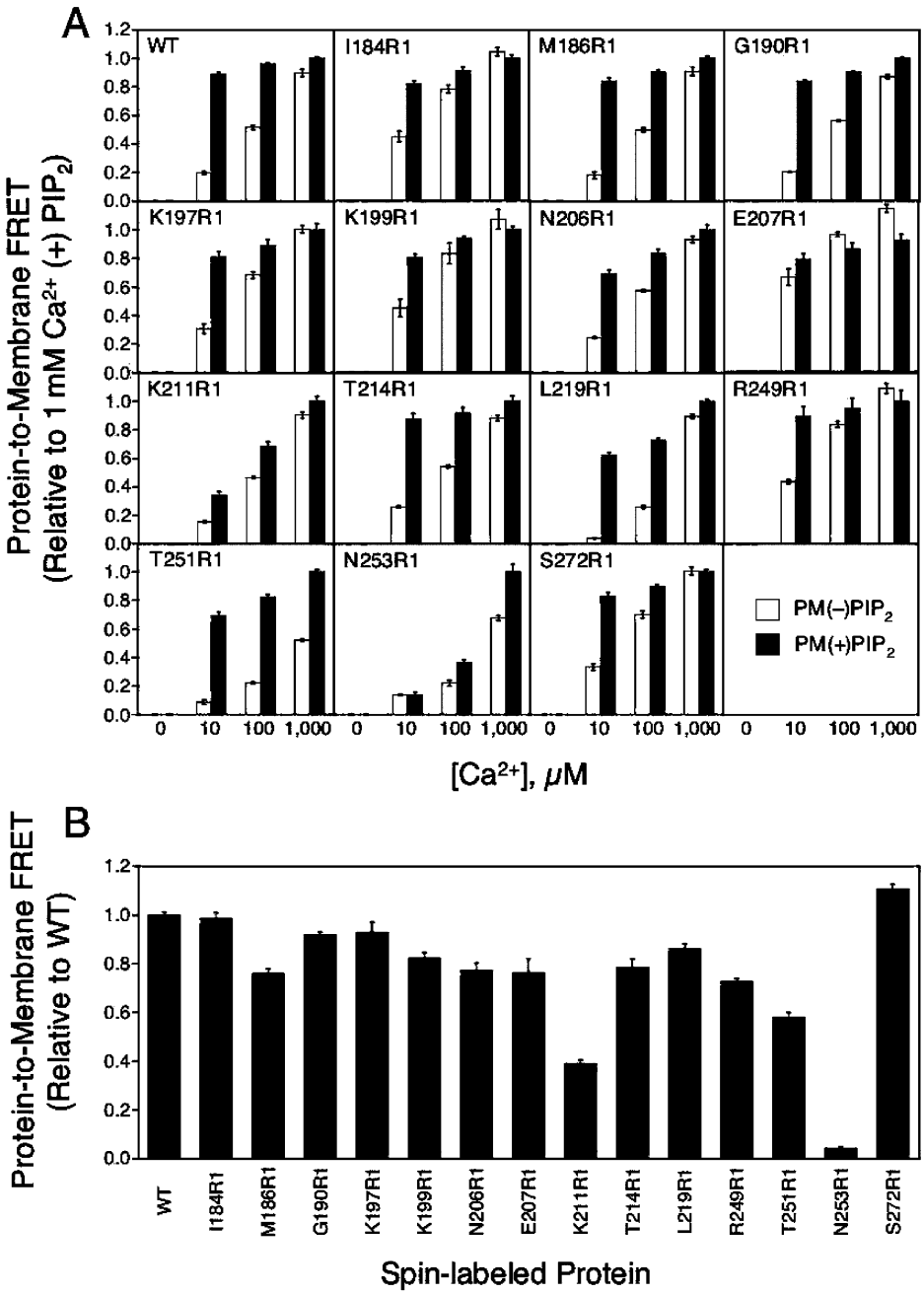

FIGURE 2: Effect of spin-labeling on Ca^{2+}-dependent membrane binding. (A) Protein-to-membrane FRET assay to measure the PIP_2 sensitivity of membrane binding at three different Ca^{2+} concentrations (10, 100, and 1000 μM), carried out as described in Materials and Methods using sonicated unilamellar vesicles (SUVs) composed of physiological lipid mixtures containing PS, and either lacking or containing PIP_2. Data for each spin-labeled domain are normalized to the protein-to-membrane FRET value obtained for membranes containing PIP_2 in the presence of 1000 μM Ca^{2+}. (B) Total binding of spin-labeled domains to physiological membranes containing PS and PIP_2 in the presence of 10 μM Ca^{2+}, relative to the binding observed for the wild type C2 domain. Experimental conditions for (A) and (B): 0.2 μM protein and 200 μM total lipid in 25 mM HEPES, 140 mM KCl, 15 mM NaCl, 0.5 mM $MgCl_2$, 0.15 mM EDTA (as a Ca^{2+} buffer), pH 7.4, 25 °C. Sufficient Ca^{2+} was added to generate the indicated free Ca^{2+} concentrations. Table 1 summarizes the lipid compositions of the membranes used in these experiments, which are designed to mimic the composition of the plasma membrane inner leaflet, either lacking or containing the native level of PIP_2.

used in protein-to-membrane FRET measurements by monitoring FRET from 3 intrinsic, donor tryptophans in the C2 domain to the acceptor dansyl-PE-containing membranes, which yields sensitive, specific detection of membrane docking (*38, 39*). Table 1 presents the lipid mole ratios of both the PM(−)PIP_2 and PM(+)PIP_2 membranes.

Figure 2 summarizes the results of these binding studies. Figure 2A analyzes the ability of each modified PKCα C2 domain to recognize and bind PIP_2 as a target lipid. The data indicate that wild type, unmodified C2 domain exhibits a 4-fold increase in membrane binding when the lipid mixture contains PIP_2 at 10 μM Ca^{2+}, corresponding to a 20-fold affinity enhancement, in excellent agreement with the 21-fold value measured previously (*24*). In the present study, spin-labeled mutant domains are operationally defined as possessing a nativelike PIP_2 interaction if inclusion of PIP_2 generates at least a 2-fold increase in membrane binding at 10 μM Ca^{2+}. Figure 2B compares the total membrane binding of wild type and mutant domains under conditions requiring simultaneous recognition of Ca^{2+}, PS and PIP_2 for normal

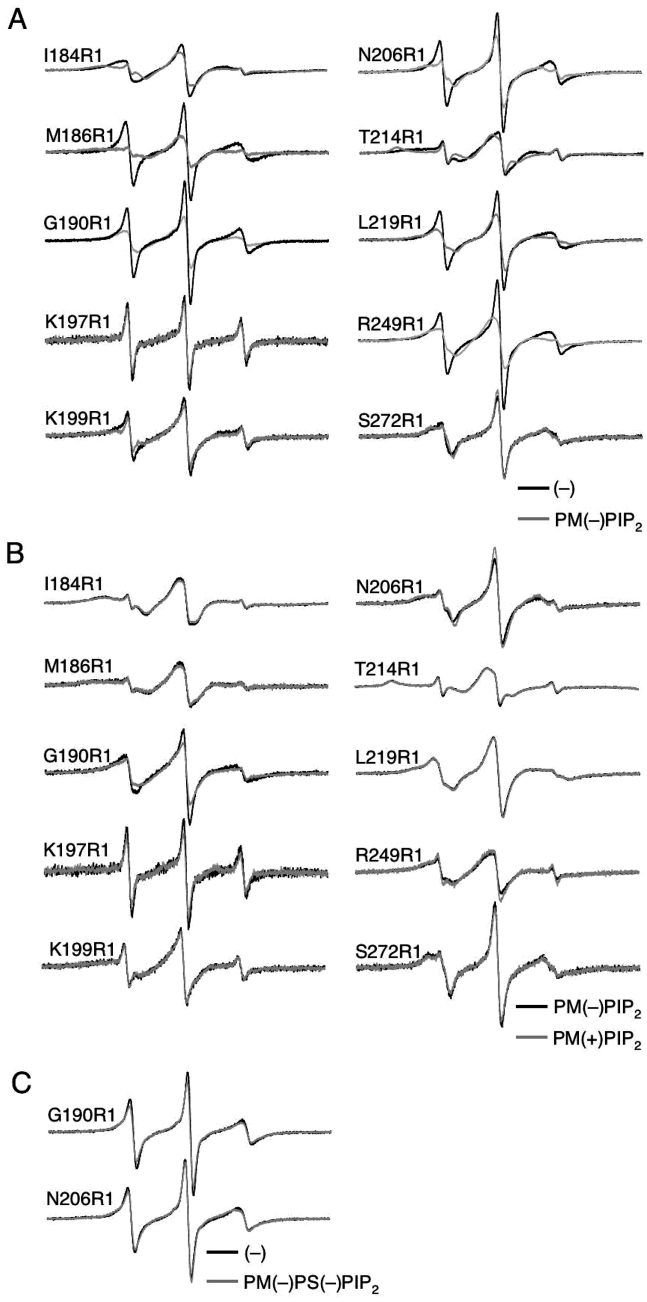

FIGURE 3: Effects of membrane docking on the EPR spectra of spin-labeled C2 domains. (A) EPR spectra for the 10 functional spin-labeled mutants acquired in the presence of Ca^{2+} either without membranes (black line) or with physiological membranes containing PS but lacking PIP_2 (gray line). (B) EPR spectra for the same spin-label mutants in the presence of Ca^{2+} and physiological membranes containing PS and either lacking (black line) or containing PIP_2 (gray line). (C) EPR spectra for G190R1 and N206R1 in the presence of Ca^{2+} either without membranes (black line) or with membranes lacking both PS and PIP_2 (gray line), showing that membrane docking is specific and does not occur in the absence of both target lipids. Spectra were acquired at 23 °C, and samples contained 10−200 μM protein, 1 mM Ca^{2+}, and 0 or 40 mM total lipid as SUVs in 25 mM HEPES, 140 mM KCl, 15 mM NaCl, 0.5 mM $MgCl_2$, pH 7.4. For (A) and (B), membrane composition as in Table 1; for (C), membrane composition as in Table 1 except that both PS and PIP_2 are replaced with PE.

docking. Here, spin-labeled mutant domains are operationally defined as possessing nativelike total membrane binding if they exhibit no more than a 30% change in membrane binding relative to the wild type domain under these conditions.

Of the 14 spin-labeled C2 domains, 10 exhibit native, or near-native, PIP_2-sensitivities and total membrane binding levels (Figure 2). These 10 functional variants yield at least a 2-fold increase in membrane binding when PIP_2 is included in the lipid mixture, and also display total membrane binding differing no more than 30% from the wild type value under conditions requiring simultaneous binding of Ca^{2+}, PS and PIP_2. The remaining 4 perturbed variants exhibit larger deviations from native function: (i) N253R1 located in Ca^{2+}- and PS-binding loop 3 almost completely eliminates membrane docking, presumably due to loss of essential PS interactions; (ii) K211R1 in the PIP_2 binding site reduces total membrane binding by 60% and significantly inhibits PIP_2 recognition; (iii) T251R1 in Ca^{2+}- and PS-binding loop 3 reduces membrane binding by 40% but retains normal PIP_2 recognition, suggesting a modest effect on PS affinity; and (iv) E207R1 in the PIP_2 binding site significantly perturbs PIP_2 recognition but retains near normal membrane binding, suggesting that neutralization of the native E207 side chain may counteract the free energy cost of reduced PIP_2 binding. Interestingly, in contrast to the perturbing effects of K211R1, modifications of 2 other lysines in the PIP_2 binding site, K197R1 or K199R1, retain near-native PIP_2 recognition. This observation is consistent with previous work demonstrating that K209 and K211 are more critical for specific PIP_2 binding than K197 and K199 (*22*). Thus, the cluster of 4 lysines believed to directly contact PIP_2 is robust toward substitution at certain positions, and 3 lysines can be sufficient for PIP_2 recognition as long as these include K209 and K211.

The 4 spin-label modifications operationally identified as perturbing were not employed further in the present study, despite the fact that these 4 variants retain high levels of membrane docking under EPR conditions, where elevated concentrations of Ca^{2+}, membrane and C2 domain strongly drive the equilibrium toward the membrane-docked state. The membrane binding assays (Figure 2) reveal that, for each of these 4 variants, one of the two lipid binding sites is seriously damaged. Even when the remaining native lipid binding site is sufficient for membrane docking under EPR conditions, the structure of the membrane docked state is likely to be perturbed by the damaged lipid binding site. Thus, subsequent EPR studies focused on the 10 functional spin-labeled proteins. Figure 1B illustrates the locations of these functional spin-labels in 3 regions: (i) the Ca^{2+} and membrane binding loops (I184R1, M186R1, G190R1, T214R1, L219R1, and R249R1); (ii) the PIP_2 binding site (K197R1, K199R1, and N206R1); and (iii) a distal, control region not involved in membrane docking (S272R1). Some of these 10 functional spin-labeled mutants exhibit minor perturbations (Figure 2), but they all retain either native or near-native binding sites for Ca^{2+}, PS and PIP_2, and they all dock to membranes under conditions where docking requires simultaneous binding of target lipids at both lipid binding sites. Such dual target lipid binding at 2 distinct lipid binding sites is a defining feature of the native C2 domain, thus the 10 functional variants likely retain a native or near-native membrane docking geometry suitable for EPR analysis. Moreover, these 10 variants ensure a sufficient number of final EPR distance constraints to accurately define the docking geometry.

Effects of Membrane Docking and PIP_2 on EPR Spectra. We next examined the effects of physiological membrane docking on the EPR spectra of spin-labeled PKCα C2

domains, both for membranes lacking and containing PIP_2. The resulting spectral changes help identify the spin-label positions that interact most strongly, on a qualitative level, with the membrane. To carry out this analysis, EPR spectra were acquired for each of the 10 functional spin-labeled C2 domains in three states: (i) Ca^{2+}-occupied, (ii) Ca^{2+}-occupied and bound to membranes containing PS, but lacking PIP_2, and (iii) Ca^{2+}-occupied and bound to membranes containing both PS and PIP_2. EPR measurements were carried out using protein and lipid concentrations that yielded docking of nearly all proteins to the membrane, with an average distance of 80 Å or more between membrane-docked C2 domains, thereby ensuring negligible spin−spin broadening. Thus, all line broadenings triggered by membrane docking can be attributed to protein-membrane interactions.

Figure 3A shows that, upon docking to membranes containing PS but lacking PIP_2, the majority of spin-labels exhibit increased spectral line width, or line broadening, characteristic of a loss of spin-label mobility. Such line broadenings are typically observed for spin-labeled lipid binding proteins that associate with membranes (*30–32, 34, 35*). Any spin-label coupled to the protein may exhibit line broadening upon membrane docking due to loss of global protein tumbling, but line broadenings are typically largest for spin-label side chains that directly contact the bilayer (*30–32, 34*). Such membrane contacts can impose steric constraints and environmental changes on the spin-label side chain, arising from (i) bound or immobilized lipids in contact with the protein, or (ii) a change in solvent environment, which in some cases can drive the spin-label side chain to associate more strongly with the protein surface. Here, the largest membrane-induced line broadenings are observed for 5 positions on the Ca^{2+}- and membrane-binding loops (I184R1, M186R1, G190R1, L219R1, and R249R1), and for 1 position (N206R1) located at the tip of the $\beta3$-$\beta4$ loop in the PIP_2 binding pocket. The observed line broadenings are consistent with previous fluorescence and EPR evidence that the CMBLs directly contact the membrane bilayer (*37*), and also suggest a direct interaction between the $\beta3$-$\beta4$ loop and the membrane, even in the absence of PIP_2. By contrast, residues K197R1, K199R1 and S272R1 display reproducible but small spectral changes upon membrane docking, suggesting that these spectral changes are due to loss of global protein tumbling rather than direct membrane contacts. K197R1 and K199R1 are located at the bottom of the concave PIP_2 binding pocket, where their interaction with the membrane may well be weak relative to N206R1 located on the rim of the binding pocket (Figure 1). Similarly, residue S272R1 is located on the opposite side of the C2 domain where it has no opportunity to contact the membrane in the membrane-docked state.

Figure 3B compares pairs of spectra for C2 domains docked to membranes containing PS, and either lacking or containing PIP_2. Quantitative difference spectra (not shown), as well as visual inspection of the spectral pairs, reveal that the PIP_2-triggered spectral changes are largest for a subset of 4 probes: G190R1, K197R1, N206R1, and R249R1. These 4 PIP_2-triggered spectral changes are fully reproducible, but are smaller in magnitude than those observed for the binding of free domain to membrane (Figure 3A). The smaller magnitudes of the PIP_2-induced spectral changes support the idea that, once the C2 domain is docked to the membrane, the binding of PIP_2 to the membrane-docked protein triggers only small changes in local spin-label mobility or environment at a subset of spin-label positions.

Overall, the spectral changes observed upon docking to physiological membranes lacking or containing PIP_2 (Figures 3A,B) arise from the specific binding of the C2 domain to one or both of its membrane-associated target lipids. No membrane binding, nor spectral changes, are observed when the membranes lack both PS and PIP_2, as illustrated in Figure 3C for representative spin-labeled proteins. When the C2 domain is docked to membranes containing the target lipid PS, the binding of the target lipid PIP_2 alters the structure of the protein−membrane complex, thereby triggering spectral changes at 4 spin-label positions scattered across the entire membrane docking face. The fact that these spectral changes are delocalized, rather than being localized in the PIP_2 binding site, suggests that PIP_2 binding to the membrane-docked C2 domain may trigger a global change in membrane docking geometry.

Effects of Membrane Docking and PIP_2 on Membrane Depth Parameters. Continuous-wave EPR power saturation was used to measure membrane depth parameters for spin-labeled C2 domains bound to physiological membranes lacking and containing PIP_2. This method measures the accessibility of the R1 label to localized paramagnetic relaxing agents that partition preferentially into the membrane hydrocarbon and aqueous phases (*27–33*). Collisions with paramagnetic agents enhance spin-label relaxation rates, and thus can be detected as an increase in the power necessary to saturate the EPR signal. To measure the depth parameter, EPR power saturation measurements were carried out for each spin-labeled protein bound to membranes in 3 otherwise identical samples: (i) containing ambient dissolved levels of the paramagnetic species O_2, (ii) purged with N_2 to remove O_2, but containing the added paramagnetic Ni^{2+} complex NiEDDA, and (iii) purged with N_2 to remove O_2, and lacking any added paramagnetic agents. For each condition, the measured half-saturation power and line width was used to calculate an accessibility parameter directly proportional to the collision rate with O_2 or NiEDDA, yielding $\Pi(O_2)$ or Π(NiEDDA), respectively (see Materials and Methods, eq 2). Since apolar O_2 preferentially partitions into the hydrophobic membrane interior, while the zwitterionic NiEDDA complex remains largely in polar regions, spin-labels exposed to the membrane and aqueous environments exhibit high O_2 and NiEDDA accessibility parameters, respectively. The depth parameter Φ is defined by the ratio of the O_2 and NiEDDA accessibilities $\{\Phi = \ln [\Pi(O_2)/\Pi(\text{NiEDDA})]\}$ (see Materials and Methods, eq 3). Positive depth parameter values indicate membrane burial with high O_2 accessibility, and negative values indicate aqueous exposure with high NiEDDA accessibility.

Figure 4 shows the relationship between the measured accessibility parameters ($\Pi(O_2)$, Π(NiEDDA)) and the depth parameter (Φ) for PKCα C2 domain docked to membranes lacking and containing PIP_2. For both types of membrane, the O_2 accessibility is relatively constant, while the NiEDDA accessibility varies over at least a 5-fold larger range and is thus primarily responsible for defining the range of the depth parameter. The observed magnitudes and dynamic ranges of the accessibility parameters suggest that the spin-labels are located primarily in the headgroup and aqueous regions

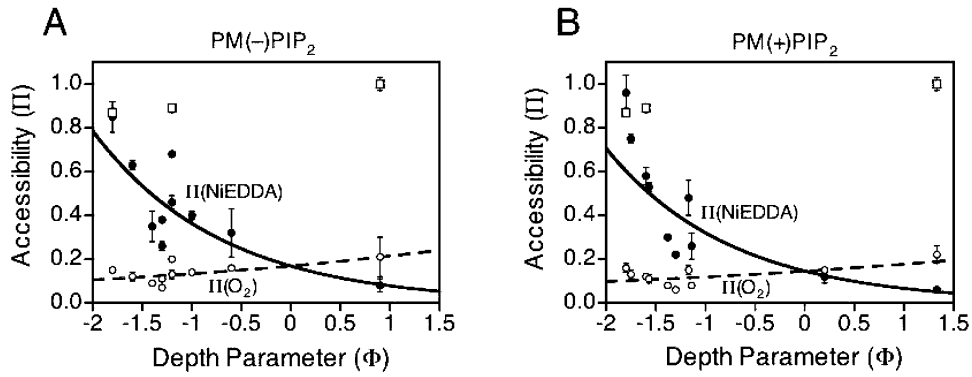

FIGURE 4: Relationship between EPR accessibility and depth parameters. Shown are the NiEDDA and O_2 accessibility parameters (Π(NiEDDA) closed circles, $\Pi(O_2)$ open circles), each plotted against the depth parameter (Φ), where all parameters were measured as described in Materials and Methods and Results. The plots reveal the larger dynamic range of the NiEDDA accessibility relative to O_2 accessibility, indicating that the depth parameter is defined largely by the NiEDDA collision rate. As a control, NiEDDA accessibility parameters were also measured in the absence of membranes (open squares) for positions N206R1, R249R1, and S272R1. For N206R1 and R249R1 on the membrane docking face, the Π(NiEDDA) values are significantly higher in the absence of membranes, indicating that membrane docking greatly slows the NiEDDA collision rate with these spin-labels. For S272R1 located distal to the membrane docking face, the presence of membranes has no significant effect on the Π(NiEDDA) value, as expected. Error bars are propagated from nonlinear least-squares best fits of power saturation data ($n \geq 15$ power settings; see eqs 2, 3), except for G190R1, K197R1, N206R1, and R249R1, for which the error bars are standard deviations of triplicate experiments ($n \geq 15$ power settings for each of the triplicate experiments). EPR and sample parameters as in Figure 3A,B legend.

Table 2: Depth parameter measurements for spin-labeled PKCα C2 domains bound to physiological membranes lacking or containing PIP_2

spin-label position	membranes	Φ	ΔΦ
I184R1	PM(−)PIP_2	−1.3 ± 0.1	−0.1
(CBL1)	PM(+)PIP_2	−1.4 ± 0.1	
M186R1	PM(−)PIP_2	−1.4 ± 0.2	+0.3
(CBL1)	PM(+)PIP_2	−1.1 ± 0.2	
G190R1[a]	PM(−)PIP_2	−1.0 ± 0.1	+1.2
(CBL1)	PM(+)PIP_2	0.2 ± 0.2	
K197R1[a]	PM(−)PIP_2	−0.6 ± 0.4	−0.6
(β3 strand)	PM(+)PIP_2	−1.2 ± 0.1	
K199R1	PM(−)PIP_2	−1.6 ± 0.3	−0.2
(β3 strand)	PM(+)PIP_2	−1.8 ± 0.2	
N206R1[a]	PM(−)PIP_2	−1.2 ± 0.1	−0.4
(3/4 loop)	PM(+)PIP_2	−1.6 ± 0.1	
T214R1	PM(−)PIP_2	−1.3 ± 0.2	0.0
(CBL2)	PM(+)PIP_2	−1.3 ± 0.2	
L219R1	PM(−)PIP_2	−1.2 ± 0.1	−0.3
(CBL2)	PM(+)PIP_2	−1.5 ± 0.2	
R249R1[a]	PM(−)PIP_2	0.9 ± 0.2	+0.4
(CBL3)	PM(+)PIP_2	1.3 ± 0.1	
S272R1	PM(−)PIP_2	−1.8 ± 0.1	0.0
(β8 strand)	PM(+)PIP_2	−1.8 ± 0.1	

Depth parameters were determined by EPR power saturation as described in Materials and Methods (eqs 1–3). Each sample contained 10−200 μM spin-labeled protein in 25 mM HEPES, 140 mM KCl, 15 mM NaCl, 0.5 mM $MgCl_2$, 1 mM Ca^{2+}, and 40 mM total lipid in the form of sonicated unilamellar vesicles; lipid composition as indicated in Table 1. Except where otherwise indicated, errors are propagated from the errors of the accessibility parameters (Π(NiEDDA) and $\Pi(O_2)$) used to calculate the depth parameter (eqs 2, 3), where $n \geq 15$ power settings were used for each accessibility parameter measurement. [a] For the indicated spin-label positions exhibiting the largest depth parameter changes, reproducibility was tested by measuring depth parameters in triplicate on different days. All were fully reproducible, and the indicated errors are standard deviations.

of the membrane, both in the absence and presence of PIP_2, and are not located in the hydrophobic membrane interior where higher O_2 accessibility parameters are typically observed (*30–32, 34*).

Table 2 summarizes the depth parameters measured for the 10 functional spin-label positions when PKCα C2 domain is docked to physiological membranes containing PS but lacking PIP_2. One spin-label on CMBL3 (R249R1) exhibits a depth parameter of +0.9 ± 0.2, which is the deepest penetration detected in this state. Three probes on CMBL1 (I184R1, M186R1, and G190R1), two on CMBL2 (T214R1 and T219R1), and two on the β3-β4 hairpin (K197R1,N206R1) exhibit depth parameters in the range −0.5 to −1.4, indicating that these positions are also located in or near the headgroup region. The negative control position S272R1 exhibits a depth parameter of −1.8 ± 0.1, consistent with its fully solvent-exposed location on the C2 domain surface opposite the membrane docking surface. Interestingly, K197R1 in the PIP_2 binding site is relatively well protected from NiEDDA collisions [Π(NiEDDA) is 4-fold smaller at this position than at the solvent exposed S272R1 position], but is highly mobile as indicated by its sharp spectrum (Figure 3). This apparent discrepancy can be rationalized by considering the location of K197R1 at the bottom of the concave PIP_2 binding cavity (Figure 1): when this cavity is docked to the membrane, the side chains on the rim could contact the membrane directly and block entry of NiEDDA into the cavity, while the side chains in the cavity could be shielded from NiEDDA even though they retain their intrinsic mobilities and are unable to reach the membrane surface.

Table 2 also compares the depth parameters measured for C2 domains docked to two different variants of the physiological lipid mixture: (i) containing only one target lipid (PS), or (ii) containing both target lipids (PS and PIP_2). This comparison reveals that PIP_2 triggers a change in the docking geometry. Four positions exhibit reproducible, PIP_2-induced depth parameter changes as determined by independent, triplicate measurements on different days. The largest change is observed for G190R1 on CMBL1, which shifts from a depth parameter of −1.0 ± 0.2 to +0.2 ± 0.2. This shift indicates that PIP_2 binding triggers deeper penetration of

CMBL1 into the headgroup region, bringing the spin-label closer to the hydrocarbon interior. Similarly, R249R1 on CMBL3 shifts from $+0.9 \pm 0.2$ to $+1.3 \pm 0.1$, indicating a displacement toward the hydrocarbon interior. In contrast, positions K197R1 and N206R1 on the $\beta3$-$\beta4$ hairpin shift from -0.6 ± 0.4 to -1.2 ± 0.1, and from -1.2 ± 0.1 to -1.6 ± 0.1, respectively, suggesting that the PIP_2 binding pocket moves further from the membrane surface upon PIP_2 binding. Although the magnitudes of these 4 depth parameter changes exhibit moderate scatter, the results of the independent, triplicate measurements indicate that the signs of the 4 changes never vary. Thus, PIP_2 always shifts the depth parameters of the two CMBL spin-labels to become more positive, and those of the two $\beta3$-$\beta4$ hairpin spin-labels to become more negative. Moreover, the depth parameter changes observed at these 4 positions are reproducibly larger in magnitude than those observed at other positions (Table 2), and the same 4 spin-labels also exhibit the largest PIP_2-induced spectral changes (Figure 3B). It follows that these 4 spin-label positions are most sensitive to the PIP_2-induced change in docking geometry. By contrast, the smaller depth parameter changes observed at the other 6 spin-label positions are within the range of experimental error.

Overall, the reproducible depth parameter changes observed at the 4 most sensitive spin-label positions strongly suggest that PIP_2 binding drives 2 spin-labels on CMBLs 1 and 3 more deeply into the membrane, while 2 spin-labels in the PIP_2 binding pocket move away from the membrane surface into solution. Qualitatively, the simplest model that explains these findings is a rigid body rotation of the C2 domain, which changes the angle of the domain long axis relative to the membrane surface.

Modeling the Membrane Docking Geometry, Including the Effect of PIP_2 Binding. In order to generate a structural model of the PKCα C2 domain docked to the surface of a physiological membrane, and the effect of PIP_2 binding on the docking geometry, we employed a previously described procedure that has been successfully applied to other membrane-bound C2 domains (*31–35*). The method begins by generating a set of calibration points which relate measured EPR depth parameters to known distances of penetration in the membrane. Subsequently, these calibration points, plus the known structure of the protein, are used to develop a self-consistent model that positions the protein in the membrane to optimize the agreement between the experimental depth parameters of individual spin-labels and the modeled locations of these spin-labels in the membrane.

To generate calibration points, we utilized EPR depth parameters measured for 4 spin-labeled lipids as previously described (*32*). Additionally, we used depth parameters measured for 2 spin-labeled mutants (M38R1 and L39R1) of the cytosolic phospholipase A_2 ($cPLA_2$) C2 domain bound to physiological membranes containing PIP_2. When depth parameters were measured both in simple 3:1 PC:PS membranes and physiological membranes, their values were the same, within error, indicating that, to a first approximation, the depth parameter is independent of membrane lipid composition. For each of the 6 spin-labeled lipids and proteins, the distance that the spin-label penetrates into the membrane is known (*27, 32, 36*), thus providing a set of 6 calibration points directly relating the EPR depth parameter to membrane penetration distances.

To prepare the known crystal structure coordinates of the PKCα C2 domain (1dsy (*16*),) for analysis of membrane docking geometry, we substituted cysteine residues at the 10 functional positions and appended the R1 spin-label via a disulfide linkage. Typically, the MTSSL side chain employed herein adopts a stable conformation hydrogen bonded to the protein backbone, as observed in crystal structures (*40*). Thus, the side chain conformation of each spin-label was adjusted to the preferred (g^+, g^+) configuration of $+300°$, $+300°$ about the first two dihedral angles (*40*), which yielded sterically acceptable conformations for 7 of the 10 spin-label positions. The remaining 3 positions (T214R1, L219R1 and R249R1) exhibited steric clashes for the (g^+, g^+) configuration, and thus their geometry was further modified by rotations about the Cα−Cβ and Cβ−Sγ bonds of the side chains to minimize clashes (see Materials and Methods). The final conformations for T214R1, L219R1 and R249R1 were (g^+, t), (g^+, t), and (t, g^+), respectively.

Finally, a self-consistent, best-fit model was developed for the membrane docking geometry using the available constraints. These included (i) the measured depth parameters and known penetration distances of the spin-labeled lipids and $cPLA_2$ C2 domain positions, (ii) the three-dimensional coordinates of the crystal structure modified as described above with the 10 spin-labeled side chains, and (iii) the measured depth parameters of the 10 spin-labeled PKCα C2 domains. The model was based on an established hyperbolic relationship between the depth parameter and the distance from the center of the membrane bilayer (*33*). Standard mathematical modeling software, Igor Pro (wavemetrics), was used to translate and tilt the C2 domain structure relative to the membrane, while optimizing the fit of the protein and lipid constraints to the hyperbolic function. Only one of the 10 spin-label positions, K197R1, failed to yield good agreement with the best-fit hyperbola, suggesting that its modeled side chain conformation might be incorrect. Thus, during subsequent optimization, the conformation of K197R1 was changed from (g^+, g^+) to (t, t), yielding improved agreement with the best-fit hyperbola. Figure 5A,B presents the final best-fit distributions of measured depth parameters as a function of membrane penetration distances, for membranes containing PS while lacking or containing PIP_2, respectively. In these plots, the penetration distance is operationally defined as the distance from a given spin-label nitrogen to the membrane plane containing the highest density of headgroup backbone phosphates (*42*). Notably, the best-fit data agree quite well with the standard hyperbolic relationship between the depth parameter and membrane penetration distance (Figure 5A,B; eqs 4, 5).

Figure 5C,D presents the two resulting optimized docking geometries for membranes lacking and containing PIP_2, while Figure 5E tests the agreement between these docking geometries and the measured depth parameter changes. In both geometries (Figure 5C,D), the color-scaled depth parameters range smoothly from reddish positions (extreme positive values) penetrating most deeply into the membrane to bluish positions (extreme negative values) exposed most highly to aqueous solvent, emphasizing the excellent fit between the measured depth parameters and the spatial locations of spin-label side chains. When the measured PIP_2-induced depth parameter changes are plotted against the predicted depth parameter changes back-calculated from the

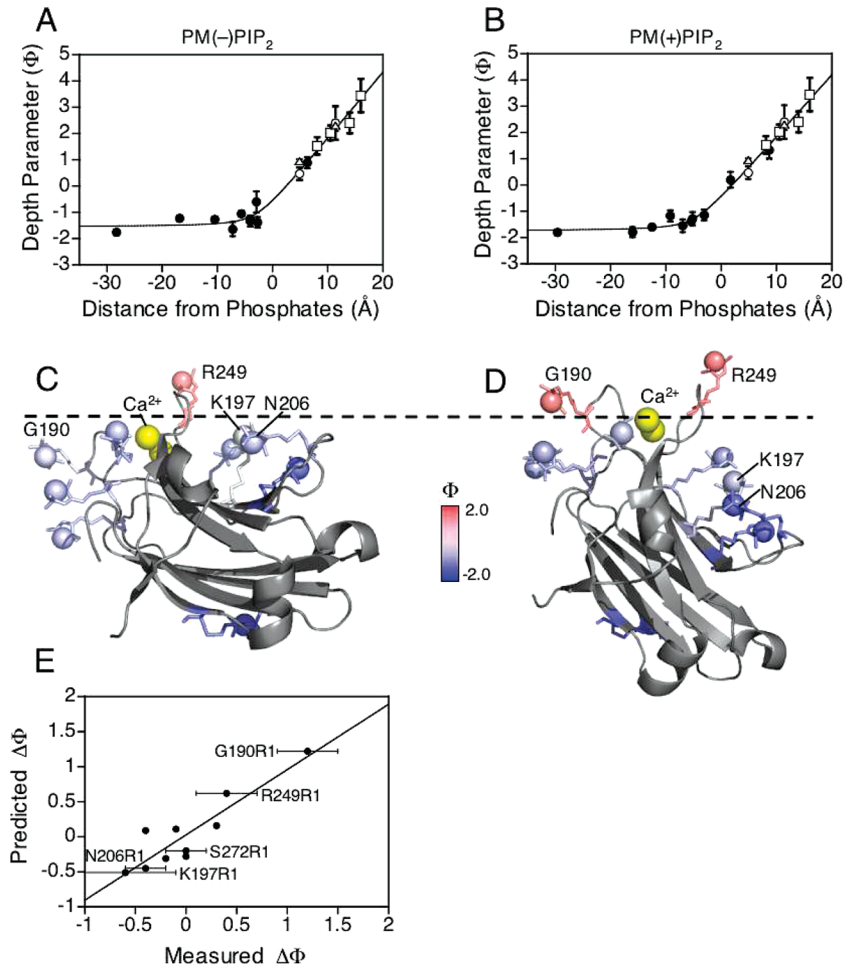

FIGURE 5: Use of EPR depth parameters to determine membrane docking geometries in the absence and presence of target lipid PIP_2. (A, B) Modeling analysis of the PKCα C2 domain docked to physiological membranes containing PS, and either lacking or containing PIP_2, was carried out as described in the text. The analysis utilized constraints provided by (i) experimental depth parameters for the functional spin-labels on the C2 domain (filled circles), and for calibration lipids (open squares) and proteins (open triangles for 3:1 PC:PS membranes, and open circles for PM(+)PIP_2 membranes), (ii) the known crystal structure of the PKCα C2 domain (*16*), and (iii) the known hyperbolic dependence of the depth parameter on the location of the spin-label in the bilayer (*33*). Shown are the two final best-fit models for C2 domain docking to membranes (A) lacking and (B) containing PIP_2, each illustrating the excellent fit between measured spin-label depth parameters and the theoretical hyperbolic relationship (solid curve, eqs 4, 5). (C, D) Depicted is the C2 domain crystal structure (1dsy) (*16*) modified with the 10 functional spin-labels as described in the text, illustrating the two docking geometries defined by the above best-fit models. Comparison of these two geometries for C2 domain docked to physiological membranes containing PS and either (C) lacking or (D) containing PIP_2 reveals that the PIP_2-induced geometry change is best described as a rigid body rotation of the C2 domain long axis toward the membrane normal. Shown also are the bilayer phosphate plane (dashed line), the bound Ca^{2+} ions (yellow spheres) and the side chain nitrogen of each spin-label (colorized sphere, where colors are scaled from red for positive, membrane-associated depth parameters to blue for negative, aqueous depth parameters). Images were rendered in Pymol (DeLano Scientific LLC). (E) Testing the best-fit, PIP_2-induced geometry change for self-consistency by plotting the depth parameter changes predicted by the two best-fit models against the measured depth parameter changes (Table 2). The data are highly linear, exhibiting a unitary slope (0.9 ± 0.2) and passing through the origin (0.0 ± 0.1), indicating near perfect agreement between the modeled geometry change and the experimental depth parameters. To examine the reproducibility of the experimental depth parameters, the 4 key spin-label positions exhibiting the largest PIP_2 effects (G190R1, K197R1, N206R1, R249R1) were subjected to three different measurements on different days. For these positions, the error bars indicate the resulting standard deviations, demonstrating that the depth parameters are sufficiently reproducible to accurately define the PIP_2-induced geometry change. EPR and sample parameters as in the Figure 3A,B legend.

two docking geometries, in principle the result should yield a straight line of slope of 1 passing through the origin. Indeed, Figure 5E shows that the result is linear ($R = 0.90$), exhibiting a slope of 0.9 ± 0.2 and a *y*-intercept of 0.0 ± 0.1, indicating excellent agreement between (i) the PIP_2-induced geometry change defined by the two docking models and (ii) the experimental, PIP_2-induced depth parameter changes.

Figure 6 analyzes these two docking models in more detail by inserting the two best-fit docking geometries into a modeled lipid bilayer. Examination of the two docking geometries indicates that PIP_2 has little or no effect on the overall membrane penetration depth of the C2 domain: in the model lacking PIP_2 the two bound Ca^{2+} ions are located at depths −3 ± 3 Å and −5 ± 3 Å, respectively, from the phosphate plane while the presence of PIP_2 shifts the Ca^{2+} ions to 0 ± 2 Å and −2 ± 2 Å, respectively. Thus any effect of PIP_2 on the depth of the Ca^{2+} ions is smaller than the experimental uncertainty (±3 Å). The uncertainty here is greater than previously observed (±1 Å) in an analogous EPR study of the membrane-docked C2 domain of cytosolic phospholipase C2 (cPLA2), due to the fact that the relatively shallow penetration of the PKCα C2 domain into the headgroup region yielded only 1 positive depth parameter

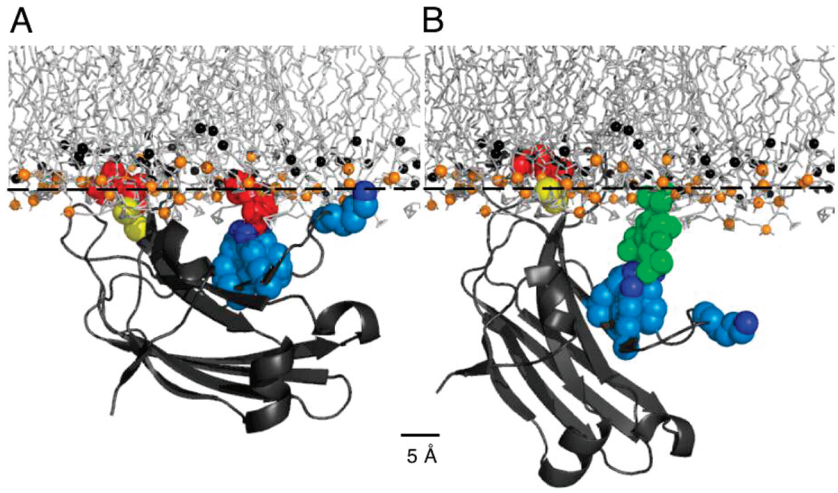

FIGURE 6: Best-fit membrane docking geometries calculated for PKCα C2 domain in the absence and presence of target lipid PIP_2. Shown are models of the two best-fit C2 domain geometries embedded in a model lipid bilayer lacking (A) or containing (B) PIP_2. In both models, the two Ca^{2+} ions (yellow spheres) bound to the CMBLs are directly contacting a PS headgroup (red spheres) in the phosphate plane (dashed line; phosphate atoms are orange spheres, and the carbonyl oxygens are black spheres). Shown also are the lysine cluster (K197, K199, K209, K211) and a fifth lysine (K205) on the β3-β4 hairpin (blue spheres with dark blue terminal nitrogen). (A) In the absence of PIP_2, the lysine cluster K197, K199, K209, and K211 binds a PS headgroup (*21, 22, 41*) and the fifth lysine K205 contacts the membrane surface. (B) In the presence of PIP_2, the larger PIP_2 headgroup (green spheres) replaces PS in the PIP_2 binding site, causing the long axis of the domain to tilt 40 ± 10° away from the membrane surface (see text) and altering the contacts between the β3-β4 hairpin and the membrane. Images generated in Pymol (DeLano Scientific LLC) using the PKCα-C2 domain crystal structure (1dsy (*16*),), a simulated POPC bilayer (popc128a (*45*)), and a PIP_2 headgroup from the PLCδ1-PH domain crystal structure (1mai (*46*)).

on its docking face, while the considerably deeper penetration of the $cPLA_2$ C2 domain into the hydrocarbon core yielded positive depth parameters at 9 probe positions. Such positive depth parameters significantly enhance the precision of penetration distances, due to the strong dependence of depth parameter on distance in this limit (see Figure 5A,B). Notably, both of the PKCα C2 domain docking models (Figure 6) place the two Ca^{2+} ions near the phosphate plane of the bilayer, as previously observed for the two Ca^{2+} ions of membrane-docked $cPLA_2$ C2 domain. The proximity of the Ca^{2+} ions to the anionic phosphate plane makes good sense in a simple electrostatic picture of protein-membrane interaction.

The major effect of PIP_2 on the docking geometry of the PKCα C2 domain is to change the docking angle of the domain relative to the bilayer plane. Specifically, in the presence of PIP_2, the β3-β4 hairpin defining the PIP_2 binding site (and thus the entire β-sandwich core of the domain) adopts an angle more perpendicular to the membrane surface. The pivot point for this rotation lies near the bound Ca^{2+} ions and is closest to the α-carbon of P194, such that CMBL1 penetrates more deeply into the headgroup region while the PIP_2 binding site moves away from the membrane surface. In order to quantitate the membrane docking angle of the C2 domain a vector, oriented nearly parallel to the domain long axis, was defined from Ca^{2+} ion 501 to the α-carbon of N206 on the β3-β4 hairpin. The binding of the C2 domain to PIP_2 causes a rigid body rotation, which causes the angle between the defined vector and the membrane plane to increase 40 ± 10°. The simplest interpretation of this rotation is that, in both the absence and presence of PIP_2, the Ca^{2+} ions are firmly coordinated to PS, thereby defining the pivot point for domain rotations. Finally, Figure 6 includes modeled PS and PIP_2 headgroups to test whether the different sizes of these target lipids are well-accommodated by the two docking geometries. In the absence of PIP_2, both the CMBL and β3-β4 hairpin sites are adequately filled by the small anionic headgroup of PS when the long axis of the C2 domain is nearly parallel to the membrane surface (Figure 6A). By contrast, the much larger PIP_2 headgroup (*12*) cannot be accommodated by its binding site in this docking geometry; instead, the C2 domain must rotate the lysine cluster away from the membrane surface to bind PIP_2 (Figure 6B). The transformations required to generate both docking geometries from the crystal structure coordinates (1dsy) are detailed in Materials and Methods.

DISCUSSION

Use of EPR Site-Directed Spin-Labeling to Analyze Membrane Docking Geometry: Assumptions. The present study utilizes site-directed spin-labeling to probe the structure of the protein−membrane complex formed by the docking of PKCα C2 domain to a physiological lipid bilayer designed to mimic the lipid composition of the plasma membrane inner leaflet. In addition, the effect of PIP_2 binding on the docking geometry is examined. In general, the use of site-directed spin-labeling to probe membrane docking geometry relies on three key assumptions: (I) that the spin-labels utilized do not significantly perturb the protein−membrane interaction, (II) that the backbone structure of the protein does not change significantly upon membrane docking, and (III) that the side chain conformations of the spin-labels generally conform to the most common geometry observed in crystal structures (*40*).

In the present study, assumption I is satisfied because only those spin-label positions which retain native or near-native membrane binding are used in EPR studies. These functional spin-label modifications, representing 70% of the spin-label positions tested, retain functional binding sites for Ca^{2+}, and for the target lipids PS and PIP_2. The fact that only 30% of the spin-label positions tested yield major perturbations of membrane binding is consistent with previous observations that the protein−membrane interactions of peripheral proteins

Table 3: Thermodynamic Contributions of PIP_2 and PS to the Ca^{2+} Dependent Membrane Docking of PKCα C2 Domain

membranes	$[Ca^{2+}]_{1/2}$[a] (μM)	$\Delta\Delta G$[b] (RT)
PM [(−)PIP_2(−)PS]	350 ± 50	
PM [(−)PIP_2(+)PS]	33 ± 7	− 2.4 ± 0.2
PM [(+)PIP_2(−)PS]	12 ± 3	− 3.4 ± 0.2
PM [(+)PIP_2(+)PS]	1.6 ± 0.1	− 5.4 ± 0.1

[a] Previously reported $[Ca^{2+}]_{1/2}$ values measured for PKCα C2 docking to physiological membranes lacking or containing the target lipids PIP_2 and PS. Two of the lipid compositions were the same as those in Table 1 (PM[(−)PIP_2(+)PS] = PM(−)PIP_2; PM[(+)PIP_2(+)PS] = PM(+)PIP_2) (*24*). The other two lipid compositions were derived from those in Table 1 by substituting all PS with PE. [b] $\Delta\Delta G$ relative to the PM [(−)PIP_2(−)PS] value. Errors are propagated from the errors of each absolute $[Ca^{2+}]_{1/2}$.

are plastic and robust, such that EPR spin-labels can be introduced at most docking surface positions with little or no loss of function (*31, 32, 34, 35*).

The present evidence strongly indicates that assumptions II and III are also satisfied, since the crystallographic backbone structure of PKCα C2 domain incorporating the standard (g^+, g^+) geometry of the spin-labels at the majority of sites, coupled with the EPR data, together yield self-consistent structural models for the protein docked to 2 different types of membrane. In particular, the backbone structure provided by crystallographic analysis of the isolated, Ca^{2+}-occupied C2 domain provides an excellent fit of the experimental EPR depth parameters to the known hyperbolic relationship between depth parameter and distance of penetration into the membrane: no changes to the crystal structure backbone are needed to optimize this hyperbolic fit, either in the absence or presence of PIP_2. The simplest interpretation of these findings is that the Ca^{2+}-occupied C2 domain possesses a relatively rigid backbone structure, especially in the two regions that directly contact membrane: the Ca^{2+}- and membrane-binding loops (CMBLs), and the PIP_2 binding site. The rigidity of the CMBLs is provided by the two bound Ca^{2+} ions which form multiple coordination bonds to each CMBL (*16*), thereby generating a noncovalent but strong, multivalent framework stabilizing CMBL structure. Such Ca^{2+}-generated structural stability has also been observed for the CMBLs of the $cPLA_2$ C2 domain (*32, 43*). By contrast, the backbone rigidity of the PIP_2 binding site is proposed to arise from its location on the $\beta3$-$\beta4$ hairpin, which is part of the rigid β-sandwich that forms the core of this and other C2 domains (*3*). Finally, both of the self-consistent structural models described herein employed the (g^+, g^+) side chain geometry at most spin-label positions, as in prior self-consistent structural models generated by spin-label EPR studies (*30–32, 34, 35*). Thus, the present findings are consistent with the current view that the (g^+, g^+) geometry is the most prevalent conformation of the MTSSL side chain (*40*).

PKCα C2 Domain Possesses Two Distinct Target Lipid Binding Sites. Recently it has been demonstrated that PKCα C2 domain requires interactions with two target phospholipids, PS and PIP_2, in order to dock to the plasma membrane surface at physiological Ca^{2+} concentrations (*22–24*). The binding of these two target lipids involves two independent binding sites: (i) the CMBLs bind Ca^{2+} and PS, but not PIP_2, while (ii) the $\beta3$-$\beta4$ hairpin binds either PS or PIP_2 (*14, 15, 22, 24, 41*). Table 3 presents the previously published $[Ca^{2+}]_{1/2}$ values for the docking of PKCα C2 domain to membranes composed of physiological lipid mixtures containing both PS and PIP_2, or lacking them in different combinations. The table also presents the corresponding $\Delta\Delta G$ values for these docking reactions, relative to the free energy change associated with docking to membranes lacking both PS and PIP_2. The $\Delta\Delta G$ values indicate that the binding free energies of PS and PIP_2 both contribute to the total free energy of Ca^{2+}-triggered binding to physiological membranes, indicating that the C2 domain interacts simultaneously with both lipids when bound to the membrane surface. The observation that the free energy change for binding to membranes containing both target lipids ($\Delta\Delta G = -5.4$ RT) may be smaller than expected for the additive binding of the two target lipids at independent sites ($\Delta\Delta G = -5.8$ RT) is consistent with the conclusion that the $\beta3$-$\beta4$ hairpin can bind PS when the higher affinity ligand PIP_2 is unavailable (*22, 24, 26*), such that PIP_2 binding often competitively displaces a bound PS rather than filling an empty site.

Docking Geometries of PKCα C2 Domain Bound to Target Membranes Lacking and Containing PIP_2. The structural basis of PKCα C2 domain binding simultaneously to both PS and PIP_2 on a bilayer surface has remained largely undefined, since limited structural information has been available for the membrane-docked C2 domain, and no such information has been available for membranes containing both target lipids. The present study analyzes the docking geometries of PKCα C2 domain bound to physiological membranes possessing lipid mixtures approximating those of the plasma membrane inner leaflet. One type of membrane contains the target lipid PS but not PIP_2, (very crowded) while a second type contains both PS and PIP_2 at physiological mole fractions. Evidence provided by EPR spectral changes, depth parameter measurements, and modeling results together reveal that when bound to membranes lacking PIP_2, the C2 domain exhibits a docking geometry consistent with the simultaneous binding of PS at both the CMBL and $\beta3$-$\beta4$ hairpin sites. (This docking geometry yields significantly greater contact between the $\beta3$-$\beta4$ hairpin and the membrane than our lower resolution model previously determined for a smaller density of spin-labeling sites (*37*); compare Figures 1A and 5C). When docked to membrane also containing PIP_2, the docking geometry is significantly different. Specifically, the CMBL site remains anchored to its bound PS in the headgroup layer of the membrane, while the binding of the larger PIP_2 to the $\beta3$-$\beta4$ hairpin drives a rotation of the domain long axis toward an angle more normal to the membrane surface (Figure 6). To analyze the evidence for these two docking geometries, it is simplest to separately discuss the findings for the CMBL and $\beta3$-$\beta4$ hairpin binding sites.

(i) The PS-binding CMBLs penetrate deeply into the headgroup layer, but little or not at all into the hydrocarbon layer, both in the absence and in the presence of PIP_2, as indicated by 5 lines of evidence. First, large EPR spectral line broadenings, arising from spin-label mobility losses or environmental changes, are observed upon membrane docking for positions on each of the three CMBLs (Figure 3A). Similar line broadenings have previously been observed for spin-labels on other C2 domains, predominantly for spin-label positions that directly contact or penetrate the bilayer (*30–32, 34, 35*). Second, EPR depth parameters

measured for one or more spin-labels on each CMBL are significantly more positive than that observed for the control aqueous position, indicating that these spin-labels indeed penetrate into the membrane (Table 2). The values of these depth parameters fall within the range previously observed for spin-labels exposed to the headgroup region of the bilayer (*32*). Third, when the measured depth parameters (together with lipid and protein spin-label calibration points) are used to build a structural model of the membrane-docked C2 domain, excellent fits are obtained between the experimental data and the well-established hyperbolic form of the depth parameter (Figure 5). These best-fit data sets yield self-consistent structural models for the membrane-docked C2 domain in the absence and presence of PIP_2 (Figures 5, 6). In both cases, the CMBLs penetrate into the headgroup layer with the 2 bound Ca^{2+} ions positioned, within error, at or near the headgroup phosphate plane. Fourth, electrostatics have been shown to play a central role in C2 domain docking to membranes (*44*), and the present docking models are consistent with the simple electrostatic notion that the positively charged Ca^{2+} ions will lie near the anionic phosphate plane (*32, 33*). Moreover, these models account for the direct coordination of the Ca^{2+} ions by PS phosphate oxygens observed in the crystal structure of the protein−PS complex (*16*). Fifth, PIP_2 binding reproducibly perturbs the EPR spectrum and increases the burial depth of only 2 CMBL spin-labels (G190R1, R249R1), while the 4 other CMBL positions exhibit spectra and depth parameters which are unaltered, within error (Figure 3, Table 2). Overall, it follows that the CMBLs of the membrane-docked C2 domain are anchored in the headgroup layer, both in the absence and in the presence of PIP_2. When PIP_2 binds to the C2 domain, the CMBLs are repositioned slightly, consistent with the idea that PIP_2 causes a rigid domain rotation about an axis lying nearby the Ca^{2+} ions. As a result, spin-labels on the membrane-penetrating tips of the CMBLs, such as G190R1 and R249R1 on CMBLs 1 and 3, respectively, move slightly deeper into the headgroup region upon PIP_2 binding.

(ii) The PIP_2 binding site on the $\beta3$-$\beta4$ hairpin can directly contact either the PS or PIP_2 target lipid headgroups. In the absence of PIP_2 the site binds PS, but the binding of the larger PIP_2 headgroup (*12*) pushes the site away from the membrane surface and thus triggers a rigid body rotation of the C2 domain as indicated by four lines of evidence. First, considering C2 domain docking to membrane lacking PIP_2, spectral changes indicate that the spin-label at the tip of the $\beta3$-$\beta4$ hairpin (N206R1) contacts the membrane surface. By contrast the two probes at positions within the lysine cluster (K197R1, K199R1) do not exhibit significant mobility changes upon membrane docking, consistent with their positions deeper in the concave site where their contact with the membrane would be minimal. Second, the probe at the hairpin tip (N206R1) and one of the lysine cluster probes (K197R1) exhibit depth parameters significantly more positive than the aqueous control position, indicating that they lie at or near the membrane surface, where they would be protected from collisions with the large, aqueous probe NiEDDA. Third, when PIP_2 binds to the membrane-docked C2 domain, the spin-label at the hairpin tip (N206R1) undergoes a significant increase in mobility, suggesting that the probe has moved out of contact with the membrane. Fourth, both this probe and one of the lysine cluster probes (K197R1) exhibit significantly more negative depth parameters upon PIP_2 binding, arguing that these positions both move into more aqueous environments where they are more accessible to NiEDDA.

Previous findings also support the idea that the lipid binding site on the $\beta3$-$\beta4$ hairpin lies in direct contact with PS in the absence of PIP_2. Neutralization of lysine pairs within the $\beta3$-$\beta4$ lysine cluster yields a 2−3-fold loss of affinity for 3:1 PC:PS membranes, indicating that the cluster possesses significant membrane interactions even in the absence of PIP_2 (*22*). Stoichiometry measurements indicate that PKCα C2 domain binds at least 2 PS molecules (*41*), and direct binding of a PS headgroup analogue to the lysine cluster has been observed by crystallography (*26*). Thus, when the C2 domain is docked to membranes lacking PIP_2, the association between the lysine cluster and PS pulls the PIP_2 binding site into membrane contact. However, when the significantly larger PIP_2 headgroup occupies the site, it pushes the site away from the membrane surface, thereby exposing the lysine cluster and hairpin tip to solution while burying parts of CMBL1 more deeply in the membrane.

To better define these two different docking geometries, a modeling analysis was carried out based on constraints provided by (i) experimental depth parameters for the functional spin-labels on the C2 domain, and for calibration lipids and proteins possessing spin-labels at known membrane depths, (ii) the known crystal structure of the PKCα C2 domain (*16*), and (iii) the previously described hyperbolic relationship between the depth parameter and the membrane penetration depth (*33*). The resulting best-fit models of the two docking geometries are characterized by excellent agreement between the measured depth parameters and the known hyperbolic dependence of the depth parameter on membrane penetration depth (Figures 5A,B). Moreover, these models are fully self-consistent with the known structure of the C2 domain, and with the predominant conformation of spin-label side chains, indicating that the PIP_2-induced change in docking geometry is best described as a rigid body rotation of the C2 domain. Specifically, the long axis of the C2 domain tilts 40 ± 10° toward the membrane normal, as illustrated in Figure 6. Finally, EPR spin-label methods have been successfully applied to the analysis of signal-induced structural changes in transmembrane proteins (*47–49*). The present study shows that the site-directed EPR spin-label can also be used to analyze signal-induced changes in the docking geometries of peripheral membrane proteins.

Biological Implications. In the native cellular setting, it has been recently shown that the PIP_2 binding site of the PKCα C2 domain is essential for specific targeting to the plasma membrane during cytoplasmic Ca^{2+} signals (*22*). Moreover, binding of this site to its target lipid PIP_2 is essential for membrane docking at physiological Ca^{2+} concentrations (*24*). It follows that the membrane docking geometry observed herein for the C2 domain docked to PIP_2 provides the first molecular view of the structural state responsible for specific accumulation of the PKCα C2 domain on the plasma membrane during physiological Ca^{2+} signaling events.

In an activated cell, it is likely that the plasma membrane-bound population of PKCα C2 domains includes both of the membrane docking geometries described herein. Following a rapid Ca^{2+} transient, our current working model

for the kinetics of Ca^{2+} activation and membrane docking begins with binding of a single Ca^{2+} ion to the CMBLs, followed by docking of the C2 domain to the plasma membrane via association with one of the two target lipids. Either (i) the CMBLs associate with PS, the most common anionic lipid, and a second Ca^{2+} ion, or (ii) the $\beta3$-$\beta4$ hairpin site binds PIP_2 (*24*). Subsequently, a second target lipid molecule binds to yield simultaneous occupancy of both lipid binding sites and stable membrane association. As this membrane-bound domain diffuses on the bilayer surface, it likely undergoes multiple exchanges of PS molecules at its CMBL site, and both PS and PIP_2 at its $\beta3$-$\beta4$ hairpin site. The ability of one binding site to maintain membrane association during lipid exchange at the other site would significantly extend the bound state lifetime of the membrane-docked C2 domain, thereby allowing the activated PKCα kinase to phosphorylate more target proteins.

Finally, in the full-length PKCα protein the C2 domain lies between (i) the N-terminal pair of DAG-binding C1 domains and (ii) the C-terminal protein kinase domain. It is possible that the geometry change observed when PS is replaced by PIP_2 in the lysine cluster could modulate the biological activities of the other domains, thereby regulating DAG binding or protein phosphorylation. Such a possibility must be tested in the full-length protein, but, in principle, it is possible that the regulation provided by the PIP_2-induced tilting of the C2 domain could lead to different average PKC activities in regions of the plasma membrane containing different local densities of the target lipids PS and PIP_2.

ACKNOWLEDGMENT

The authors gratefully acknowledge the gift of the PKCa C2 domain expression plasmid from Drs. S. Corbalan-Garcia, A. Torrecillas, and J. C. Gomez-Fernandez (U. Murcia, Spain); as well as helpful discussions with Drs. J. A. Corbin, A. H. Erbse, J. H. Evans, and J. D. Knight (U. Colorado, Boulder).

REFERENCES

1. Nalefski, E. A., and Falke, J. J. (1996) The C2 domain calcium-binding motif: structural and functional diversity. *Protein Sci. 5*, 2375–2390.
2. Chapman, E. R., and Davis, A. F. (1998) Direct interaction of a Ca2+-binding loop of synaptotagmin with lipid bilayers. *J. Biol. Chem. 273*, 13995–14001.
3. Cho, W. (2001) Membrane targeting by C1 and C2 domains. *J. Biol. Chem. 276*, 32407–32410.
4. Hurley, J. H., and Meyer, T. (2001) Subcellular targeting by membrane lipids. *Curr. Opin. Cell Biol. 13*, 146–152.
5. DiNitto, J. P., Cronin, T. C., and Lambright, D. G. (2003) Membrane recognition and targeting by lipid-binding domains. *Sci. STKE 2003*, re16.
6. Hurley, J. H. (2006) Membrane binding domains. *Biochim. Biophys. Acta 1761*, 805–811.
7. Cho, W., and Stahelin, R. V. (2006) Membrane binding and subcellular targeting of C2 domains. *Biochim. Biophys. Acta 1761*, 838–849.
8. Hui, E., Bai, J., and Chapman, E. R. (2006) Ca2+-triggered simultaneous membrane penetration of the tandem C2-domains of synaptotagmin I. *Biophys. J. 91*, 1767–1777.
9. Nishizuka, Y. (1995) Protein kinase C and lipid signaling for sustained cellular responses. *FASEB J 9*, 484–496.
10. Dempsey, E. C., Newton, A. C., Mochly-Rosen, D., Fields, A. P., Reyland, M. E., Insel, P. A., and Messing, R. O. (2000) Protein kinase C isozymes and the regulation of diverse cell responses. *Am. J. Physiol. 279*, L429–L438.
11. Newton, A. C. (2001) Protein kinase C: structural and spatial regulation by phosphorylation, cofactors, and macromolecular interactions. *Chem Rev 101*, 2353–2364.
12. McLaughlin, S., and Murray, D. (2005) Plasma membrane phosphoinositide organization by protein electrostatics. *Nature 438*, 605–611.
13. Corbalan-Garcia, S., and Gomez-Fernandez, J. C. (2006) Protein kinase C regulatory domains: the art of decoding many different signals in membranes. *Biochim. Biophys. Acta 1761*, 633–654.
14. Medkova, M., and Cho, W. (1998) Mutagenesis of the C2 domain of protein kinase C-alpha. Differential roles of Ca2+ ligands and membrane binding residues. *J. Biol. Chem. 273*, 17544–17552.
15. Corbalan-Garcia, S., Rodriguez-Alfaro, J. A., and Gomez-Fernandez, J. C. (1999) Determination of the calcium-binding sites of the C2 domain of protein kinase Calpha that are critical for its translocation to the plasma membrane. *Biochem. J. 337* (Part 3), 513–521.
16. Verdaguer, N., Corbalan-Garcia, S., Ochoa, W. F., Fita, I., and Gomez-Fernandez, J. C. (1999) Ca(2+) bridges the C2 membrane-binding domain of protein kinase Calpha directly to phosphatidylserine. *EMBO J. 18*, 6329–6338.
17. Nalefski, E. A., Wisner, M. A., Chen, J. Z., Sprang, S. R., Fukuda, M., Mikoshiba, K., and Falke, J. J. (2001) C2 domains from different Ca2+ signaling pathways display functional and mechanistic diversity. *Biochemistry 40*, 3089–3100.
18. Conesa-Zamora, P., Lopez-Andreo, M. J., Gomez-Fernandez, J. C., and Corbalan-Garcia, S. (2001) Identification of the phosphatidylserine binding site in the C2 domain that is important for PKC alpha activation and in vivo cell localization. *Biochemistry 40*, 13898–13905.
19. Stahelin, R. V., Rafter, J. D., Das, S., and Cho, W. (2003) The molecular basis of differential subcellular localization of C2 domains of protein kinase C-alpha and group IVa cytosolic phospholipase A2. *J. Biol. Chem. 278*, 12452–12460.
20. Corbalan-Garcia, S., Garcia-Garcia, J., Rodriguez-Alfaro, J. A., and Gomez-Fernandez, J. C. (2003) A new phosphatidylinositol 4,5-bisphosphate-binding site located in the C2 domain of protein kinase Calpha. *J. Biol. Chem. 278*, 4972–4980.
21. Torrecillas, A., Laynez, J., Menendez, M., Corbalan-Garcia, S., and Gomez-Fernandez, J. C. (2004) Calorimetric study of the interaction of the C2 domains of classical protein kinase C isoenzymes with Ca2+ and phospholipids. *Biochemistry 43*, 11727–11739.
22. Evans, J. H., Murray, D., Leslie, C. C., and Falke, J. J. (2006) Specific translocation of protein kinase Calpha to the plasma membrane requires both Ca2+ and PIP2 recognition by its C2 domain. *Mol. Biol. Cell 17*, 56–66.
23. Sanchez-Bautista, S., Marin-Vicente, C., Gomez-Fernandez, J. C., and Corbalan-Garcia, S. (2006) The C2 Domain of PKCalpha Is a Ca(2+)-dependent PtdIns(4,5)P(2) Sensing Domain: A New Insight into an Old Pathway. *J. Mol. Biol. 362*, 901–914.
24. Corbin, J. A., Evans, J. H., Landgraf, K. E., and Falke, J. J. (2007) Mechanism of specific membrane targeting by C2 domains: localized pools of target lipids enhance Ca2+ affinity. *Biochemistry 46*, 4322–4336.
25. Oancea, E., and Meyer, T. (1998) Protein kinase C as a molecular machine for decoding calcium and diacylglycerol signals. *Cell 95*, 307–318.
26. Ochoa, W. F., Corbalan-Garcia, S., Eritja, R., Rodriguez-Alfaro, J. A., Gomez-Fernandez, J. C., Fita, I., and Verdaguer, N. (2002) Additional binding sites for anionic phospholipids and calcium ions in the crystal structures of complexes of the C2 domain of protein kinase calpha. *J. Mol. Biol. 320*, 277–291.
27. Altenbach, C., Greenhalgh, D. A., Khorana, H. G., and Hubbell, W. L. (1994) A collision gradient method to determine the immersion depth of nitroxides in lipid bilayers: application to spin-labeled mutants of bacteriorhodopsin. *Pro.c Natl. Acad. Sci. U.S.A. 91*, 1667–1671.
28. Yu, Y. G., Thorgeirsson, T. E., and Shin, Y. K. (1994) Topology of an amphiphilic mitochondrial signal sequence in the membrane-inserted state: a spin labeling study. *Biochemistry 33*, 14221–14226.
29. Ball, A., Nielsen, R., Gelb, M. H., and Robinson, B. H. (1999) Interfacial membrane docking of cytosolic phospholipase A2 C2 domain using electrostatic potential-modulated spin relaxation magnetic resonance. *Proc. Natl. Acad. Sci. U.S.A. 96*, 6637–6642.
30. Frazier, A. A., Wisner, M. A., Malmberg, N. J., Victor, K. G., Fanucci, G. E., Nalefski, E. A., Falke, J. J., and Cafiso, D. S. (2002) Membrane orientation and position of the C2 domain from cPLA2 by site-directed spin labeling. *Biochemistry 41*, 6282–6292.

31. Frazier, A. A., Roller, C. R., Havelka, J. J., Hinderliter, A., and Cafiso, D. S. (2003) Membrane-bound orientation and position of the synaptotagmin I C2A domain by site-directed spin labeling. *Biochemistry 42*, 96–105.
32. Malmberg, N. J., Van Buskirk, D. R., and Falke, J. J. (2003) Membrane-docking loops of the cPLA2 C2 domain: detailed structural analysis of the protein-membrane interface via site-directed spin-labeling. *Biochemistry 42*, 13227–13240.
33. Malmberg, N. J., and Falke, J. J. (2005) Use of EPR power saturation to analyze the membrane-docking geometries of peripheral proteins: applications to C2 domains. *Annu. Rev. Biophys. Biomol. Struct. 34*, 71–90.
34. Rufener, E., Frazier, A. A., Wieser, C. M., Hinderliter, A., and Cafiso, D. S. (2005) Membrane-bound orientation and position of the synaptotagmin C2B domain determined by site-directed spin labeling. *Biochemistry 44*, 18–28.
35. Herrick, D. Z., Sterbling, S., Rasch, K. A., Hinderliter, A., and Cafiso, D. S. (2006) Position of synaptotagmin I at the membrane interface: cooperative interactions of tandem C2 domains. *Biochemistry 45*, 9668–9674.
36. Jaud, S., Tobias, D. J., Falke, J. J., and White, S. H. (2007) Self-induced docking site of a deeply embedded peripheral membrane protein. *Biophys. J. 92*, 517–524.
37. Kohout, S. C., Corbalan-Garcia, S., Gomez-Fernandez, J. C., and Falke, J. J. (2003) C2 domain of protein kinase calpha: elucidation of the membrane docking surface by site-directed fluorescence and spin labeling. *Biochemistry 42*, 1254–1265.
38. Nalefski, E. A., Slazas, M. M., and Falke, J. J. (1997) Ca^{2+}-signaling cycle of a membrane-docking C2 domain. *Biochemistry 36*, 12011–12018.
39. Nalefski, E. A., and Falke, J. J. (2002) Use of fluorescence resonance energy transfer to monitor Ca(2+)-triggered membrane docking of C2 domains. *Methods Mol. Biol. 172*, 295–303.
40. Langen, R., Oh, K. J., Cascio, D., and Hubbell, W. L. (2000) Crystal structures of spin labeled T4 lysozyme mutants: implications for the interpretation of EPR spectra in terms of structure. *Biochemistry 39*, 8396–8405.
41. Kohout, S. C., Corbalan-Garcia, S., Torrecillas, A., Gomez-Fernandez, J. C., and Falke, J. J. (2002) C2 domains of protein kinase C isoforms alpha, beta, and gamma: activation parameters and calcium stoichiometries of the membrane-bound state. *Biochemistry 41*, 11411–11424.
42. Wiener, M. C., and White, S. H. (1992) Structure of a fluid dioleoylphosphatidylcholine bilayer determined by joint refinement of x-ray and neutron diffraction data. III. Complete structure. *Biophys. J. 61*, 434–447.
43. Perisic, O., Fong, S., Lynch, D. E., Bycroft, M., and Williams, R. L. (1998) Crystal structure of a calcium-phospholipid binding domain from cytosolic phospholipase A_2. *J. Biol. Chem. 273*, 1596–1604.
44. Murray, D., and Honig, B. (2002) Electrostatic control of the membrane targeting of C2 domains. *Mol. Cell 9*, 145–154.
45. Hoff, B., Strandberg, E., Ulrich, A. S., Tieleman, D. P., and Posten, C. (2005) 2H-NMR study and molecular dynamics simulation of the location, alignment, and mobility of pyrene in POPC bilayers. *Biophys. J. 88*, 1818–1827.
46. Ferguson, K. M., Lemmon, M. A., Schlessinger, J., and Sigler, P. B. (1995) Structure of the high affinity complex of inositol trisphosphate with a phospholipase C pleckstrin homology domain. *Cell 83*, 1037–1046.
47. Hubbell, W. L., Cafiso, D. S., and Altenbach, C. (2000) Identifying conformational changes with site-directed spin labeling. *Nat. Struct. Biol. 7*, 735–739.
48. Perozo, E., and Rees, D. C. (2003) Structure and mechanism in prokaryotic mechanosensitive channels. *Curr. Opin. Struct. Biol. 13*, 432–442.
49. Zhang, Y., and Shin, Y. K. (2006) Transmembrane organization of yeast-syntaxin analogue Sso1p. *Biochemistry 45*, 4713–4781.
50. Vance, D. E., and Vance, J. E. (2002) *Biochemistry of Lipids, Lipoproteins, and Membranes*, Elsevier Science, Burlington, MA.
51. Roth, M. G. (2004) Phosphoinositides in constitutive membrane traffic. *Physiol. Rev. 84*, 699–730.

BI800711T